# Image cues for perceiving depth of transparent and reflective objects

# (光沢と透明物体の奥行き知覚に寄与する画像特徴量の解明)

January 2022

Doctor of Philosophy (Engineering)

Masakazu Ohara

大原　正和

Toyohashi University of Technology

別紙４－１（課程博士（英文））

Date of Submission（month day, year）: January 7th, 2022

| Department of Computer Science and Engineering | Student ID Number | D153315 |
|---|---|---|
| Applicant's name | Masakazu Ohara | |

| Supervisors | Kowa Koida<br>Michiteru Kitazaki |
|---|---|

# Abstract（Doctor）

| Title of Thesis | Image cues for perceiving depth of transparent and reflective objects |
|---|---|

Approx. 800 words


Perceiving the shape of objects in depth is an essential visual function in daily life. The human visual system tries to decompose a retinal image into the experiences of shape, motion (if it exists), illumination, and surface optics. However, this process is not always perfect, especially when no binocular cue is given, because this decomposition is an ill-posed problem. For this problem, a mis-perception of shape sometimes accompanies the mis-perception of a surface's optics, such as glossiness and albedo. It is also known that perceived depth of objects is modulated by the surface's optics. These complicated interactions between the shape and surface optics of objects is not an inherent perceptual error of the visual system, but rather, indicates the perceptual inference that is most likely occur. Recent studies have found those mis-perception associated with specular reflectance is still poorly understood in other important optical properties – transparency. Here, I focused on two important surface optics; specularity and transparency and examined how these optical properties affect human perception of three-dimensional shape. If some biases exist in perception, I ask what image features could explain any resulting depth perception.

Firstly, I examined how the human observers estimate the depth of the three-dimensional objects which were simulated to have different materials by using computer graphics. The rendered objects varied in the thickness, bumpiness, motion, transparency, specular reflectivity under photorealistic lightning environments. Observers were asked to rate the overall convexity of these objects along the depth axis. The results showed that observers perceived solid purely transparent objects as flatter than the same objects rendered with opaque (matte or specular) reflectance properties. These results were consistent across changes in thickness, bumpiness, lighting environments, and dynamic/static stimulus presentations.

Secondly, I tested how the relative intensity of specular reflection to the transparent objects affect depth perception. In the previous experiment, I found that the stimulus image of 50% specular and 50% transparent objects induced similar depth perception to the 100% specular objects. Thus, it is important to know which ratio of specular reflection contributes to a threshold change depth perception. In this experiment, various ratios of specular

reflections of transparent objects were presented. The observers compared the overall thickness along the depth axis of the transparent objects with a textured matte object. The results showed that adding only a small ratio (< 5%) of specular reflection to the refractive component was required for equating perceived thickness in depth of the matte object, and the ratio was almost equal to the specular ratio of the ordinary glass and ice. However, this specular ratio was very different across the light fields, indicating that the structure of illumination significantly biased the perceived shape of shiny transparent objects relative to matte opaque objects.

Finally, I investigated what image cues explaining those observed depth perceptions. Across the models I tested, a regional variation in local root-mean-square (vRMS) contrast of the image was shown to provide good prediction of perceived depth of the objects. The vRMS contrast is a simple second-order image statistic, and thus easy to compute from the image and maybe implementable in the human visual system. I also showed that the vRMS contrast could be applicable to shapes other than a perfect sphere.

The finding of underestimation of the perceived depth of the transparent objects, along with the overestimation of the specular objects, is particularly important in the field of material perception. Many studies of material perception have focused on the perception of the material itself, such as glossiness (related to reflective light) and transparency (related to refractive light). In my study however, I examined how shape perception was modulated by reflective/refractive optical properties. This experimental paradigm used in my study is also applicable to other material properties, including semi-transparency, chromaticity, and other complex materials.

It was also shown that perceived depth can be explained by vRMS contrast regardless of the materials, including matte, glossy, and transparent materials. Thus, many complex surfaces could be reproduced by combining relevant image-based information together. Although further examination of the model and perception is needed, the model of vRMS contrast would be helpful for industry applications that need to control the appearance of products. If the industry stakeholder wants to modify the appearance of the shape by changing surface coating and printing, the vRMS contrast model could be a good index to this end.

## Contents

# 1. Introduction

## 1.1. Surface materials in daily life and research motivation

The world around us contains objects with 3d shape and material properties (Figure 1.1). Metal and ceramic have shiny/glossy highlights. Water and glass are transparent. Clothes have various kinds of texture. Industrial gadgets, such as smartphones, have not only glossy metal bodies but also transparent parts such as camera lens and a glass cover window. People sometimes enjoy changing their appearance by putting cases and covers on them. These compounds of materials give rise to an aesthetic visual appearance.

The appearance of material is one of the most important factors influencing sales. In the case of smartphones, it has been reported that the appearance of the device contributed more to sales than the quality of its functions (DMMLab, 2016). Some reporters have shown that the appearance of the package, not its contents, also contributed to sales (Tobitani et al., 2021). In the case of automobiles, improvements in appearance of surfaces are thought to be important in parallel with improvements in the primary functions, such as the ability to drive and its fuel efficiency (Yuzawa and Yoshida, 2014; LEE et al., 2018). Thus, the research related to appearance is socially and economically important.

Figure 1.1: Many kinds of surface.

The appearance of materials does not come from materials' optical properties alone. For example, the shape of a specular highlight would be determined by both reflectance and three-dimensional shape of object. Some cosmeticians apply make-up on faces to generate favorable skin tone and sometimes in ways that modify apparent shape. When people take a picture of some objects, paying attention to surrounding environment and lighting leads to

better results. Thus, material perception is not limited to the material's optical properties, but also relates to the object's shape and its surrounding lighting environment.

Applying makeup to the skin is a primitive way to obtain good looks. In recently days, cosmetics are needed not only for their beautifying and skin protection effects, but also for improving the apparent surface shape of skin (Kawashima and Hikima, 2015). Good skin appearance accompanies change the perceptual shape. For example, face wrinkles can be hidden, the lips look fuller, and the nose and other parts are modified as intended by the makeup artist (Kao Corporation, 2020). This modification is attained not only by adding shade but also by specular reflectance. A painted shading may work under a congruent lighting environment, but may look unnatural under another incongruent lighting. Namely, the natural shading depends on the light source, in contrast, painted shadings is independent of changes in the light source. This difference generates unnatural appearance of 3d shape. To solve this problem in the makeup industry, apparent skin bumpiness is modified by adjusting the intensity of gloss in addition to shading to avoid be unnatural looks (Hashimoto, 2020). This kind of manipulation of the lightness and gloss is widely used to change shape perception. In other words, in order to study the appearance of material properties, it is important to understand its relationship of surface optics to the object's 3d shape.

It is known that considering the properties of the light source (i.e., position, intensity, direction) is important to generate a good appearance of objects. In one case, strong point-light sources are used to emphasize the luster of precious stones and precious metals. In another case, indirect lighting, which illuminates an object from wide area of the environment is used to express the softness of fabrics and skin. For a more complicated example, it is known that just before sunset is "the golden hour" for filming cars. This time is known as the time when an object's surface generates nice shading and warm and cool color gradations (Brown, 2016; Ascher, 2019). Thus, the technique of making the surface appearance favorable by adjusting the lighting is widely practiced.

Shape, material, and lighting are physical factors that affect the formation of the image of an object. When one of these factors are modified, the appearance of the other factors can also change. Despite the complex relationship between these factors, humans easily and reliably perceive three-dimensional shape and materials of ordinary objects. How does the human visual system understand the three-dimensional shape and materials of objects from their retinal images? To this end, it is important to understand how human observers tend to perceive and misperceive object shape and materials under various illuminations. How do

these percepts relate to the image cues? In this study, I performed psychophysical experiments to measure shape perception of the objects for a variety of materials and under various lighting conditions. Then I examined which image cues explain the perception of three-dimensional shapes.

## 1.2. How we perceive an object from image cues

Retinal images are informative of the surrounding illumination, shape and surface materials of an object (Figure 1.2). We try to understand the external world by decomposing the retinal image into perceptual elements through visual information processing. However, it is known that this decomposition is sometimes incorrect.

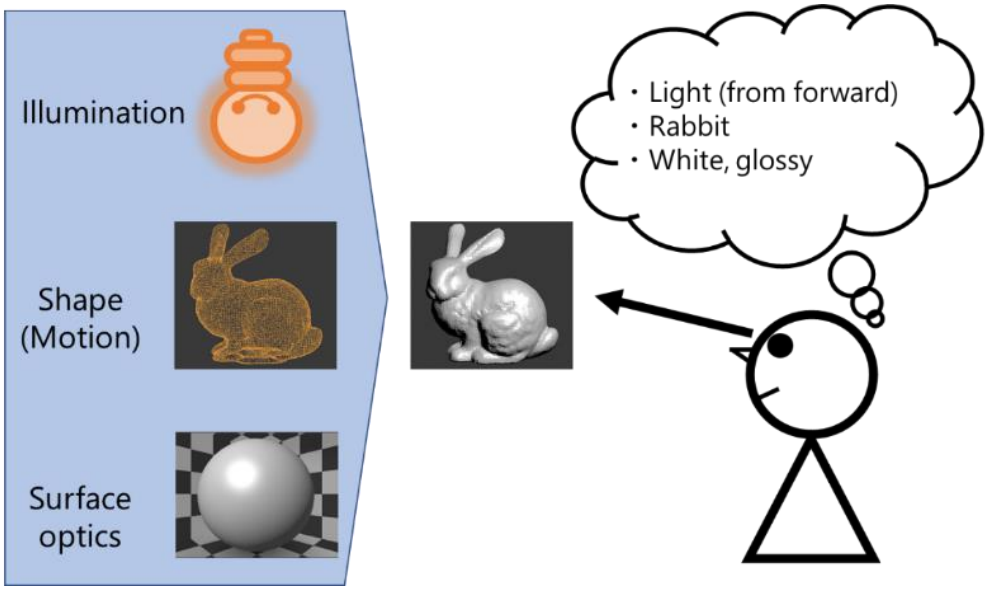


Figure 1.2: Human visual system tries to decompose a retinal image into physics-related factors. Those factors in this example are that the global illumination comes from forward top, and shape of a rabbit, and gray and glossy surface properties.

The retinal images do not always have sufficient cues. The missing information are interpolated by the observers' estimation based on their experiences. This estimation usually works well but does not always match to the external physical components. For example, when an observer estimates three-dimensional shape of an object from monocular image, there are multiple possible shapes that can generate a correct answer (Figure 1.3). This is called the ill-posed problem. In such cases, the visual system prefers the most isotropic shape from contour (Marr, 1982).

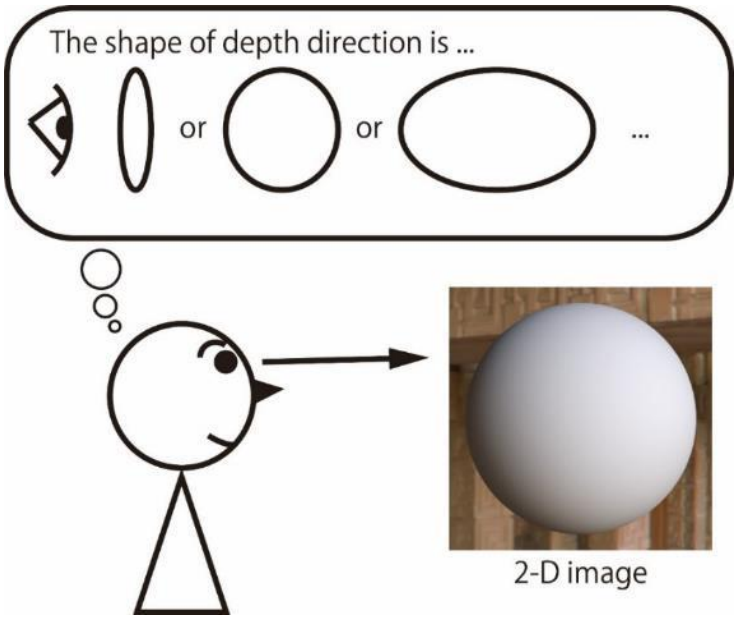


Figure 1.3: Shape estimation from two-dimensional image. In the absence of sufficient information, there are multiple possibilities for the shape of the object.

Both lightings and surface materials lead to estimation errors of 3D shapes as well. It is known that shading on the diffuse surface helps to perceive shape. Shading is made of a dark and bright part of an object that depends on relative angle between its surface and incident light. When an object has bright and dark areas on the surface concordant with the light source, the shape can be understood correctly (Ramachandran, 1988). This is known as shape perception from shading cues. In other words, the shape perception could be manipulated by shading because of its ill-posed problem. To solve the problem, the human visual system adopts a "light from above" assumption, and as a consequence, a convex shape with downward shading is more likely rather than a light-from-bottom illuminating a concave shape with upward shading (the left object in Figure 1.4) (Ramachandran, 1988).

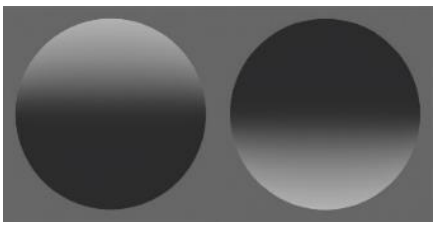

Figure 1.4: Gray spheres with shading. These two spheres have the same global shape. The difference is the position of spotlight source (left: upward, right: downward). This figure is adapted from Ramachandran (1988)

Most natural surfaces have a certain degree of specularity. On the specular reflections, the incident and reflected light on a surface has an equal angle from the normal of the surface. Thus, the image of specular highlights has information of the surface angle. Reflecting these physical constraints, highlights and reflections of the surrounding scene support the perception of correct 3D shape (Fleming et al., 2003, 2004, 2009; Fleming, 2014; Kim et al., 2016b). It is also known that adding specularity to an object with diffuse reflection increases the perceived thickness in depth (Mooney and Anderson, 2014; Ohara et al., 2020) (Figure 1.5).

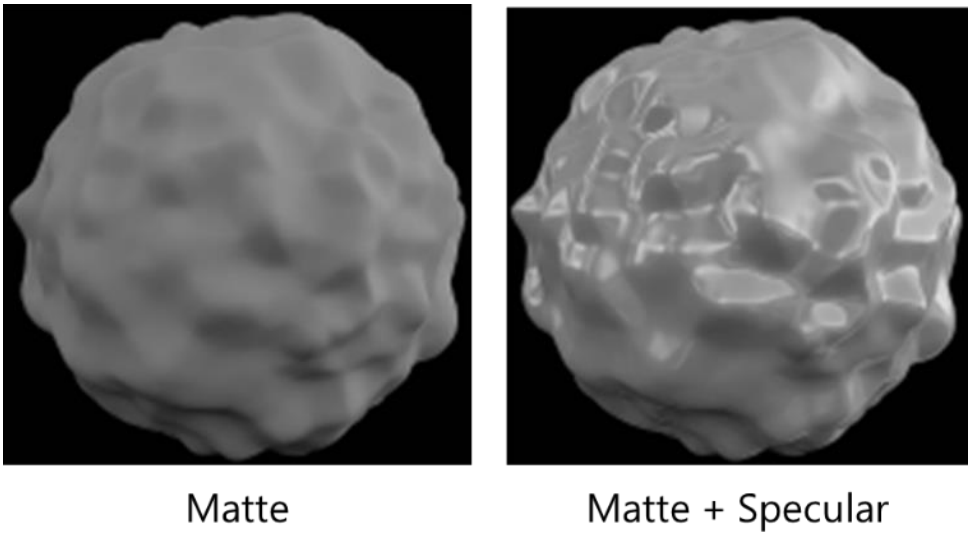


Figure 1.5: Gray bumpy objects with different surface material. These two bumpy objects have the same global shape. The left object is pure matte. The right object has added specular highlights. The object on the right appears bumpier. This figure is adopted from Figure 1 in Mooney and Anderson (2014).

Human visual system tries to solve the above mentioned ill-posed problem to understand the shape by using indirect cues, such as their contours, shading with a certain lighting direction, and specular highlights. Although the shapes, lighting directions, and optical properties are physically independent parameters, these parameters are used as indirect cues for estimating those parameters. Because each parameter has some degree of likelihood, thus prior knowledge about the likelihood of the objects could help to estimate those parameters. Those sources of prior knowledge about shapes, lighting environments, and optical properties are important characteristics of human visual information processing.

## 1.3. Refractive surface

In addition to diffuse and specular reflection, refraction is a basic property of many surface optics. In ordinary objects, these three optical properties are summed and delivered to the retina (Figure 1.6). Thus, it is important to treat all three optical properties together to understand shape and material perception.

The image of the surface of a transparent object depends on the difference in refractive index between the air and the object. In addition to the angle of the surface, the refractive image also depends on the distance between the object and background (Fleming et al., 2011b; Schlüter and Faul, 2014). This complication makes if difficult for humans to estimate the refractive index of transparent objects (Fleming et al., 2011b). Nevertheless, it is also known that perception of transparency was estimated based on the background distortion seen through transparent objects (Fleming et al., 2011b; Fleming, 2014; Todd and Norman, 2019).

The above-mentioned studies investigated how the perceived transparency of an object is evoked by its optical properties. On the other hand, transparent optical properties may affect shape perception in the same way as the specular reflection affects shape perception. There are only a few studies investigating this possibility, and they showed that shape perception of transparent objects is less accurate than that of opaque objects (Schlüter and Faul, 2019). Compared to diffuse and specular reflections (Blake and Bülthoff, 1990; Blake and Bulthoff, 1991; Fleming et al., 2004; Savarese et al., 2004a, 2004b, 2005), the effect of refractive properties on the shape perception have not been well investigated. Since diffuse, reflective, and refractive lights are all fundamental optical properties, it is a fundamental question to know the effect of transparency on shape perception.

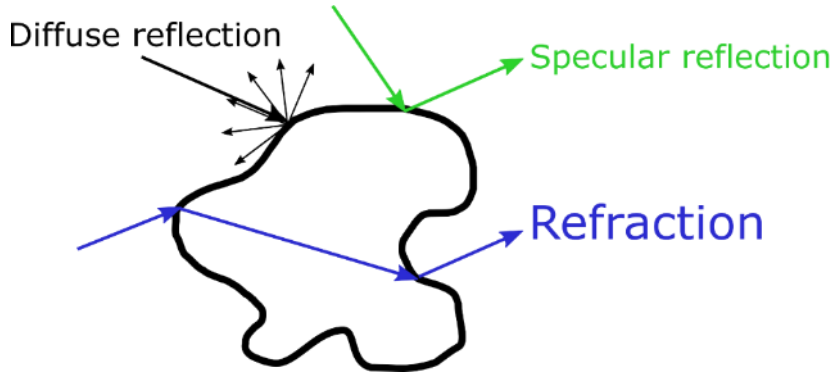


Figure 1.6: Surface optical properties focused in this study.

## 1.4. How to measure the perceived depth

There are two kinds of methods of measuring the apparent 3D shape of objects. One is a local shape task, and the other is global shape task. A typical example of the local shape task is the gauge-figure task. In the gauge-figure task, subjects are asked to indicate the direction of the normal of a certain surface, and repeated multiple points on the surface of a single object (De Haan et al., 1995; Bernhard et al., 2016). Thus, the gauge-figure task focuses on local shape of the objects. In the global shape task, there are choosing, sorting, and rating tasks. In those tasks, multiple objects are presented simultaneously or individually, and the observers view the object as a whole. Observers are asked to choose which one is thicker, to sort the objects based on their relative thickness, or to rate the objects thickness by subjective values, respectively. Thus, these tasks focus on the perception of global shape of the objects.

Which task is preferable to measure global shape perception? In the gauge-figure task, tens, or hundreds of points should be measured for each object, and finally the perceived shape for one object as a whole can be measured. If we want to compare it with other objects, we need to make similar measurements for other objects as well. In contrast, choosing, sorting, and rating tasks can easily compare the appearance of many objects, because the measurements for a single object are simpler than in the gauge-figure task. In order to compare the perceived three-dimensional shape objects with surface materials, those global tasks would be preferable.

## 1.5. Aim and approach

The world around us is full of materials including transparency, however, many complex materials are thought to be represented by a combination of diffuse reflection, glossy reflection, and transparency properties. The effect of their properties on shape perception was rather examined separately in previous studies. Thus, in this study, I consider all three optical properties together to understand shape and material perception.

Most of the research on object thickness perception has been done by comparing diffuse and specular reflective objects (Fleming et al., 2003, 2004, 2009; Fleming, 2014; Mooney and Anderson, 2014; Kim et al., 2016b), or solely on transparent objects (Schlüter and Faul, 2019). However, as seen in glass and ice, there are many situations in which transparency and glossy reflection exist together in daily life. Therefore, it is important to clarify the relationship between all three of these optical properties on the thickness perception. In this study, I assessed how the perceived thickness of objects was modulated by the three optical factors.

The human visual system attempts to estimate the three-dimensional shape of objects no matter what material they are made of. Thus, there may exist commonly applicable computation to extract shape information. In this study, I investigated image cues to perceiving thickness across three optical properties; diffuse reflection, specular reflection, and transparency. To this end, by analyzing the image of the object and the surrounding lighting environment, I report common thickness cues among different materials and global shapes.

## 2. The effect of material properties on the perceived shape of three-dimensional objects

### 2.1. Introduction

Images result from the complex interplay between illumination, surface materials, and three-dimensional (3D) shape. We perceptually untangle these complex patterns of image structure to visually infer the shape of 3D objects and their reflectance properties. However, the perceptual experience of surfaces with material properties is not always correct, and errors in perception can occur in either the recovery of a surface's material properties or 3D shape (Nishida and Shinya, 1998; Belhumeur et al., 1999; Nefs et al., 2006; Khang et al., 2007; Vangorp et al., 2007; Wendt et al., 2010; Wijntjes and Pont, 2010; Mooney and Anderson, 2014; Marlow and Anderson, 2015; Todd et al., 2015). Previous work has shown that the perceived 3D shape of opaque objects tends to be underestimated—that is, the angle between the perceived surface normal and the line of sight (Koenderink and van Doorn, 1992; De Haan et al., 1995; Todd et al., 2004; Bernhard et al., 2016). I considered how the perception of surface convexity depends on the surface optics of different materials.

Most natural surfaces have a certain degree of specularity that contributes to the perception of shape. Specular reflectance generates luminance variations in images that highly depend on the structure of the surrounding light field (Norman et al., 1995; Olkkonen and Brainard, 2011). Early work has shown that these specular reflections of the surrounding light field contribute to the perception of shape (Fleming et al., 2004). More recently, Mooney and Anderson (2014) showed that the perceived convexity of surfaces tended to be overestimated by different magnitudes depending on the simulated material composition. They found that the convexity of purely diffuse surfaces (i.e., using Lambertian shading) viewed in depth was significantly overestimated compared with ground truth. They also showed that adding sharp specular reflections using a bidirectional reflectance distribution function increased perceived convexity in excess of the surface's true curvature. These findings suggest that glossier surfaces tend to be perceived as bumpier than diffuse surfaces, and diffuse surfaces tend to be perceived as bumpier than what they are. However, increase in bumpiness of opaque surfaces can also increase the complexity and number of specular reflections and perceived surface gloss (Ho et al., 2008; Wijntjes and Pont, 2010; Marlow et al., 2012). It is possible that these complex changes in specular and diffuse shading might also influence the perception of 3D shape.

Another surface property that might influence perceived shape is the refractive nature of transparent objects. Transparent objects are abundant in daily life (e.g., water

droplets, ice, crystal). It is important to accurately perceive their 3D structure so we may interact with them. For example, we effortlessly can pick up ice from within a glass cup. These thick transparent objects have different degrees of refractive power, depending on their shape and material composition (Fleming et al., 2011b; Schlüter and Faul, 2014). Do the refractive properties of transparent surfaces influence the perception of their 3D shape?

Previous research suggests that human observers are not able to accurately estimate the refractive index (RI) of transparent objects. One study showed that perceptual judgments of transparency loosely correspond to the physical refractive indices of test objects (Fleming et al., 2011b). The researchers proposed that perception of transparency was estimated based on the background distortion seen through transparent objects (Fleming et al., 2011b; Fleming, 2014; Todd and Norman, 2019). Another study proposed that background distortions alone are not sufficient for perceiving RI because they depend on both the shape and distance of the object from the background (Schlüter and Faul, 2014). Rather than observers matching internal experiences of refractivity, these researchers found that observers tended to match surfaces directly based on similarity in image cues: specular reflections and the distortion field. Further studies have used gauge figure tasks to estimate variations in perceived surface slant (i.e., surface curvature) and found that the 3D shape of objects with semi opaque reflectance properties tends to be perceptually underestimated (Chowdhury et al., 2017; Schlüter and Faul, 2019). These interactions between perceived shape and material properties suggest that the perception of both shape and materials depends on similar sources of image-based information.

How might the visual system determine whether distortions of the light field are generated by refraction or reflection? Both shiny metallic and transparent objects reflect images of the surrounding light field that are distorted by the 3D shape of the object. A research study found that inverting an image of a solid refractive globally convex object could transform its appearance to shiny metal (Kim and Marlow, 2016). The key requirement for this material inversion effect is some consistency in the perception of shape between upright and inverted images. Normally, the inversion of the light field would only occur for metallic objects when they are concave rather than convex. The perception of a convex solid glass object with light field inversion suggests the distortions themselves provide cues to both shape and material composition. In a recent article, Tamura et al. (2018) showed that moving surfaces generate dynamic motion cues that can improve observer performance in differentiating between opaque glossy and transparent refractive materials. These perspective motion cues are likely to help observers to also infer the 3D shape of moving objects.

Here, I examined the effect of varying material properties and motion constraints on the perception of a globally convex object's 3D shape. Previous work studied the perception of curvature from diffuse and specular shading (Motoyoshi et al., 2007; Kim and Anderson, 2010; Mooney and Anderson, 2014), but perceived shape of diffusely shaded objects may differ from other surfaces with semi opaque properties (Fleming et al., 2011a; Schlüter and Faul, 2014; Chowdhury et al., 2017). Therefore, I systematically varied the simulated material composition of objects from refractive to reflective, with different amounts of specular reflectance (Figure 2.1). Observer estimates of surface convexity were then obtained to determine whether there were any variations in perceived shape from ground truth and between different material classes. This allowed me to tease apart the effects of material properties and surface motion on perceived convexity, and whether there are image cues that are predictive of the perception of shape.

## 2.2. Methods

### 2.2.1. Observers

Eight adult observers participated in the experiment, all of whom had normal or corrected-to-normal vision. The participants ranged in age from 22 to 44 years. Informed consent was obtained from all participants. Procedures were approved by the Toyohashi University of Technology ethics committee. All research was performed in accordance with the relevant guidelines and regulations.

### 2.2.2. Stimuli

All the stimuli were rendered using the open-source rendering package Blender 3D (Ver. 2.78b). The 3D geometry was created in Blender 3D by taking an initial Ico Sphere with 20,480 triangle faces and 10,242 vertices (i.e., subdivisions = 6). Bumpy surface relief was created by generating a Clouds texture (Size = 0.25, Depth = 0, Nabla = 0.03). This texture was applied to the geometry as a height map using the Displace Modifier (Midlevel = 0.5, Strength = 0.2). The Ico Sphere shape and Clouds texture and Displace Modifier are included in Blender 3D. The number of bumps along the circumference was 5–12, and its peak amplitude was 5% to 7% of the diameter of the object, based on Fourier power analyses of the radial distance of the object silhouette image (Figure 2.1A). All the stimuli were rendered with Cycles Render in Blender 3D. Cycles Render is a physically based ray tracing render engine designed for high-quality animation. The objects were rendered after they were multiplicatively scaled in depth over five levels (0.25, 0.5, 1.0, 1.5, and 2.0; hereafter referred to as *convexity*).

I rendered images without tone mapping; the intensity of the specular highlights was limited by setting the exposure, and any values exceeding the dynamic range of my standard RGB rendering were set to 255. The monitor's calibrated gamma for displaying these images was 2.2 (mean absolute error was 5.7%, measured by a color and luminance meter CS-200, Konica Minolta).

I used two light fields for rendering, either the Eucalyptus Grove or the St Peters Basilica (Figure 2.1C; source: http://www.pauldebevec.com/Probes/). There were four surface material properties: Matte, Specular, Refraction (RI = 1.51), and 50% Refraction (RI = 1.51) + 50% Specular (Figure 2.1B). I also used three sizes of 3D objects that were small, normal, or large in diameter: length of 0.5, 1.0, and 2.0 Blender Units (BU), with the corresponding display size of 6.2, 12.4, and 24.8 deg, respectively. These were made by scaling the object's shape multiplicatively equally along the X, Y, and Z directions.

The camera position was fixed to 10 BU away from the 3D object's center. Light fields were represented on a sphere with infinite diameter. Objects were oscillated sinusoidally along the horizontal axis at 1.0 Hz (amplitude = 2 BU, corresponding display size: 24.8 deg) for 5 seconds beginning from the center and moving rightwards. All movie presentations of horizontal object oscillation were rendered using a custom Python script executed in the Blender environment. All movies were rendered at 60 fps.

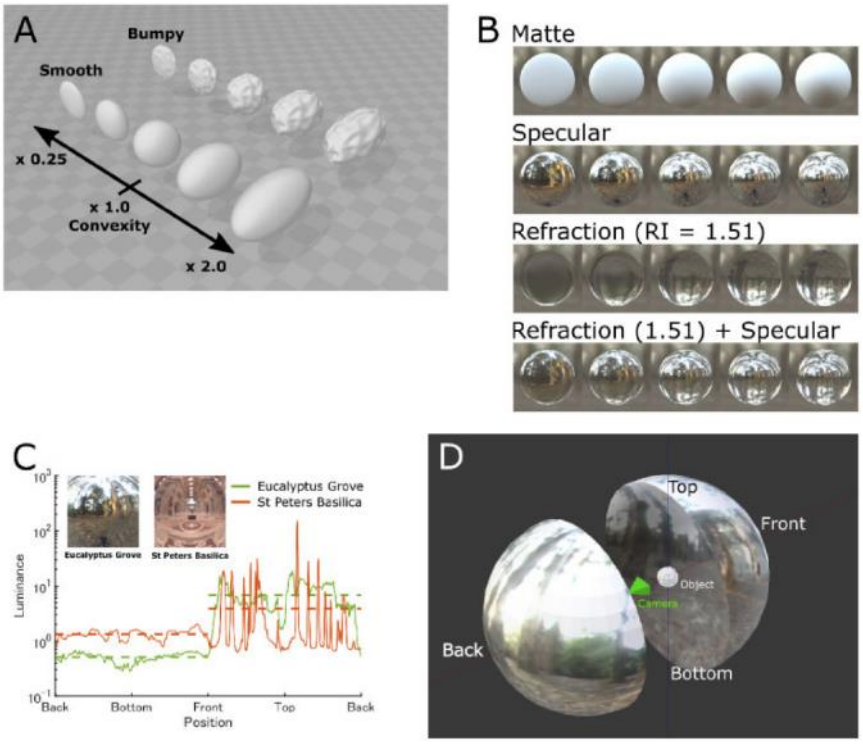


Figure 2.1: The 3D stimulus objects and environments. A: Object meshes were either smooth or bumpy and had one of five convexities in depth (range 0.25 to 2.0). The object at ?1.0 corresponds to the purely spherical surface. B: Sample renderings of smooth surfaces with different material properties which looking from the center of the object. Index of refraction for transparent objects was 1.51, equivalent to Crown glass. Matte surfaces were rendered with only diffuse reflectance. Specular conditions were rendered with only specular reflectance. C: Luminance distribution along the angle of elevation of two light fields used in this study. Luminance along the azimuth was averaged. Inset images show the central square region of the light fields. Horizontal dotted lines show the mean luminance either at top or bottom part of the light fields. D: Layout of the object, camera for rendering, and light field. A movie example can be found in Supplemental Movie

### 2.2.3. Procedure

Visual stimuli were presented using custom psychophysical software called Psymat (ver. 0.35; http://juno3d.com/software/) running on a PC (OS: Windows 10 Pro, CPU: Intel Core i7-6700, Graphic card: GeForce GTX 960).

Observers were seated, and their head fixed by a chin rest. Stimuli were presented on an LCD flat-panel display (HP E242) situated 30 cm in front of the observers. Stimulus

size was 28.6 × 28.6 cm, 51 × 51 deg, 800 × 800 pixels including the object and background of the light fields, and screen area other than the stimulus movie was gray (red = green = blue = 0.5). Observers were given a minute at the start of the experiment to practice a small number of randomly presented trials, before moving on to the formal testing session. In a block of trials, observers were shown stimulus movies for 5 seconds with both eyes open, and then they were asked to attend to the curvature of objects in depth. Participants were specifically asked to rate how flat or elongated the objects appeared on a global scale.

Following each 5-second movie presentation, the scene was replaced with a metric scale for observer ratings. The vertical bar on the left was used to indicate the length, and the oval on the right corresponds to the profile of the 3D object when it was viewed from above. The rating bar and 2D outline were modulated simultaneously when the observer pressed either the UP/DOWN arrow key to respectively increase or decrease the matched profile length. The observer was asked to report the 3D object's appearance as more elongated (like a rugby ball) or flatter (like a pancake). No feedback on their response accuracy was provided.

Once the observer was satisfied with their match, they pressed the space bar to log the response and advance to the next trial. The order of stimuli was randomized within a block of 80 conditions (4 materials × 5 convexity levels × 2 bump levels × 1 size in diameter × 2 light fields). Observers performed three repeats for each stimulus condition. On another day, observers participated in the same experiment, but the size of the objects was modified to small or large size with the order of object sizes randomly intermingled between blocks of trials.

To identify the effect of static cues on the perception of surface convexity, I presented the same stimuli statically in a follow-up experiment to determine whether there were any declines in perceptive convexity. In this follow-up experimental session, stimulus objects did not move and were presented statically at either the center, left, or right side of the stimuli locus traversed in the dynamic viewing experiment. A total of 240 randomized trials were presented to each observer (4 materials × 5 convexity levels × 2 bump levels × 2 light probes × 3 stimuli positions).

### 2.2.4. Statistical Analysis

The results were analyzed using MATLAB (Ver. R2016b). I tested for a main effect of light probe, bump level, physical convexity, and material property. The analysis of variance (ANOVA) treated physical convexity as a continuous factor but was treated as a categorical

factor in post hoc testing. The other factors were treated as categorical factors in all analyses. I also tested for interaction effects between physical convexity and material property.

## 2.3. Results

### 2.3.1. Effect of dynamic material properties on shape perception

In my first task, observers estimated the perceived convexity of moving objects with different physical convexity, bumpiness, and material properties rendered under two light fields (Figure 2.2). Perceived convexity increased significantly with physical convexity—four-way ANOVA, main effect of physical convexity: $F(1, 1919) = 1445.23$, $p < .001$, partial $\eta^2 = 0.4332$. Generally, objects with convexity larger than 1.0 (i.e., greater than spherical) were underestimated relative to ground truth, and objects with convexity smaller than 1.0 (i.e., flatter than spherical) were overestimated relative to ground truth (dashed line). Thus, the slope of perceived convexity with respect to physical convexity was smaller than the ground truth (Slope = 0.377, linear regression of all material properties). Perceived convexity also differed depending on material properties—four-way ANOVA, main effect of material properties: $F(3, 1919) = 16.91$, $p < .001$, partial $\eta^2 = 0.0262$. Across all convexity levels, objects that were purely refractive were perceived significantly flatter than specular objects of identical convexity (post hoc test, Tukey honest significance test (HSD), $p < .001$, within all other materials). The average difference in perceived convexity between the purely refractive and the other materials was approximately 0.166. A complete description of the statistics is shown in Table S1 in Supplemental Material.

The Refraction (50%) + Specular (50%) surface was perceived as comparable in convexity to the specular surface. Presumably, this occurred because the specular reflection component dominated observer's estimates of convexity. The flattest (convexity = 0.25) matte object was perceived significantly flatter than the specular object of equivalent convexity (post hoc test, Tukey HSD, $p = 0.018$).

The effect of changing material properties on perceived convexity was generally consistent across different light fields and surface bumpiness (Figure 2.2B). In all four subplots, perceived convexity significantly increased with physical convexity (post hoc test, Tukey HSD, $p < .001$, convexity = 0.25 vs. convexity = 2.0). Again, across all convexity levels in the Eucalyptus Grove light field, smooth objects that were purely refractive were perceived significantly flatter than other materials of identical convexity (post hoc test, Tukey HSD, $p < .001$, within all other materials), but not for all stimulus and viewing conditions (result shown in Table S1 in Supplemental Material). There were no significant differences between

the flattest matte object and the specular object of equivalent flatness (post hoc test, Tukey HSD, p = 0.786 [Grove–Smooth], p = 1 [Grove–Bumpy], p = 0.057 [St Peters–Smooth], p = 1 [St Peters–Bumpy]). Results were reproduced for different object sizes (Figure S1 and Table S2 in Supplemental Material).

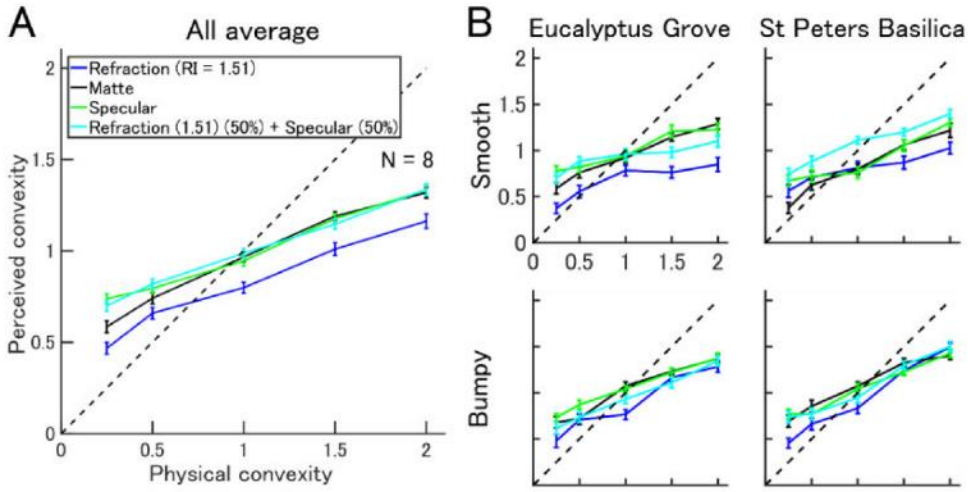


Figure 2.2: Perceived convexity for different material properties and lighting conditions for middle-sized dynamic stimuli. A: Plots show mean perceived convexity as a function of physical convexity of objects with different simulated material properties. The dashed line shows perception equating to ground truth. B: Results were shown separately by different illumination conditions and different surface bumpiness. Error bar shows standard error of mean of all trials. RI = refractive index.

### 2.3.2. Effect of perspective cue on perceived convexity

Moving objects provide several cues to infer their convexity, including motion cues and viewing perspective in addition to image cues (e.g., specular distortions). I performed another task in attempt to isolate these cues, but this time the stimuli were static images of the object placed at the center, extreme left, or extreme right of the image plane. I raise the hypothesis that looking at the sides (the left/right condition) might provide strong enough cues to shape, and then the result might be worse in the center condition and better in left/right condition.

Results are shown separately for the three positions of the object (Figure 2.3). Because left and right positions induced similar results, they were averaged. I performed a five-way ANOVA on these data to test the main effects of object position × light probe × bump level × convexity × material property. Slopes were smaller than in the motion condition, and

the slopes of the center condition were smaller than left/right conditions (slope, center = 0.102, left/right = 0.161: linear regression across all material properties). The difference between positions was not significant (five-way ANOVA, main effect of positions: $p = 0.35$). Again, I found the effect of material properties on perceived convexity ($p<.001$, details shown in Table S3 Supplemental Material). Perceived convexity increased as physical convexity increased (main effect of convexity). The flattest (convexity = 0.25) matte object was perceived significantly flatter than the specular object of equivalent convexity (post hoc test, Tukey HSD, both center and the left/right: $p < .001$). Across all convexity levels, objects that were purely refractive or purely matte were perceived significantly flatter than objects with specular reflectance and identical convexity (post hoc test, Tukey HSD: $p < .001$; Figure 2.3A and C).

These results are generally consistent across surface bumpiness and different light fields (Figure 2.3B and D). Across all convexity levels, objects that were purely refractive were perceived significantly flatter than specular objects of identical convexity except for bumpy objects in the St Peters Basilica for both the center and left/right conditions (post hoc test, Tukey HSD, $p < .001$).

It is possible these data could be explained by a learning effect because the same observers participated in the task with static images after the dynamic image task. The aforementioned hypothesis was rejected by the results; poor performance for both center and left/right, even if it had a learning effect.

The results together suggest that material properties generate static image cues for modulating the estimation of shape. However, in the absence of motion cues, the linear relationship between perceived and physical convexity was small. The decline in the slope of the relationship in the static viewing task does not appear to be due to increased uncertainty of object shape, because the error bars obtained for my perceptual estimates are similar to those of dynamic viewing tasks where a steeper slope was observed. These results suggest that dynamic and static cues contribute to the perception of shape, and these cues depend on the surface optics of different materials.

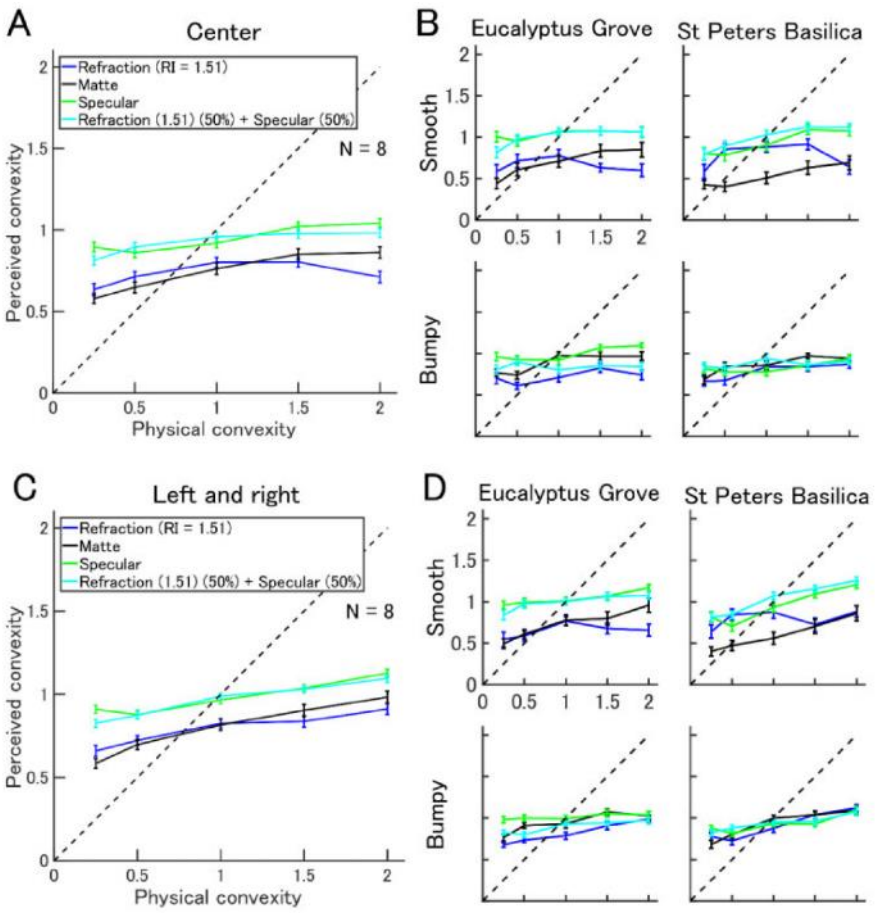


Figure 2.3: Effect of material properties on perceived convexity for static stimuli. Format is same as in Figure 2.2. A and B: Results for the object placed on center. C and D: Results for the object placed on either left or right. RI = refractive index.

### 2.3.3. Discussion

I found that an object's material properties (specular, matte, or refractive) biased its perceived convexity. Refractive and matte objects were overall perceived as flatter than the same geometry rendered with specular reflectance. Combined material properties (refractive 50% + specular 50%) were perceived as having similar shape to purely specular surfaces, indicating that the specular component dominated percepts of shape.

Consistent with previous research, specular objects were perceived as having greater relief height than matte objects of equivalent convexity (Nefs et al., 2006; Mooney and Anderson, 2014; Kim et al., 2016a). The perceived convexity of static matte objects was lower than dynamically moving objects. Motion generated percepts of shape that were closer to

veridical than the most oblique left-right static views (Wendt et al., 2010; Wilder et al., 2019). This was particularly the case for matte surfaces, which generated stronger percepts of convexity in moving simulations compared with static presentations. These findings suggest that motion provides useful optic flow information above and beyond the shape of the bounding contour alone. I also found that the perceived convexities for both matte and purely refractive objects were lower than for objects with any specular reflection. However, differences in perceived convexity were smaller for bumpy surfaces compared with smooth surfaces as indicated by the difference in the displacement of material response curves in my experiments.

Across all materials, I found that flat surfaces were generally overestimated in convexity, and elongated surfaces were underestimated in convexity. This pattern of data suggests that perceived convexity estimates of all conditions were constrained at around 1.0 (i.e., towards the appearance of a sphere). This trend might be explained by prior knowledge that objects with a circular bounding contour will tend to be spherical rather than flatter or elongated. Theoretically, 3D shape can be estimated from a 2D image in a potentially infinite number of ways, but the human visual system tends to adopt the most likely interpretation (Richards, 1988). It could also be that the objects that are compressed or elongated along the line of sight are viewed nongenetically. Thus, the observers assume isotropic spherical shape based on the likelihood, which may explain why observers tend to adopt percepts of thickness that are close to 1.0 when confronted with a circular 2D bounding contour and limited perspective information generated by material properties and/or the surrounding environment (Kunsberg and Zucker, 2014).

Why might purely refractive objects be perceived flatter than the objects with other material properties? It is known that the surface slant of transparent objects tends to be underestimated, and the result depends on a combination of transparent object properties and the surrounding environment (Schlüter and Faul, 2019). It is possible that other sources of information may be relevant (e.g., Shape from texture). Shape from texture suggests that the human visual system can estimate object shape using the distortion of textural flow across the surface. Indeed, it is known that these distortions are caused by surface shape and an object's gloss (Todd and Thaler, 2010). Similar textural gradients are provided by surfaces with relief in the form of mesostructure, which also changes scale as a function of surface orientation relative to the observer. In my static viewing conditions, I found that judgments of shape were more consistent across material properties and light fields for bumpy surfaces, presumably due to the inherent textural cues to 3D shape.

Fortunately, purely refractive objects or purely specular objects are rare in nature. Most naturally occurring objects contain surface materials with different optical components, for example, diffuse reflection, specular reflection, and refraction components including subsurface scattering. Therefore, human object shape recognition may have better accuracy when cues from diffuse and specular reflectance are added to those of transparent materials.

# 3. The role of specular reflections and illumination in the perception of thickness in solid transparent objects

## 3.1. Introduction

Images result from the complex interplay among illumination, surface's material composition, and three-dimensional (3D) shape. Although we have vivid experiences of surfaces with material properties (e.g., glossy, matte, opaque, or transparent), observers are often biased in their report of either a surface's material appearance or 3D shape (Nishida and Shinya, 1998; Belhumeur et al., 1999; Nefs et al., 2006; Khang et al., 2007; Vangorp et al., 2007; Wijntjes and Pont, 2010; Mooney and Anderson, 2014; Dövencioğlu et al., 2015; Marlow and Anderson, 2015; Todd et al., 2015). For example, previous work has shown that the perceived 3D shape of opaque objects tends to be underestimated (Koenderink and van Doorn, 1992; De Haan et al., 1995; Todd et al., 2004; Bernhard et al., 2016). However, some researchers have shown the opposite pattern of results can occur (Mooney and Anderson, 2014). Adding sharp specular reflections increased perceived convexity in excess of the surface's true curvature (Mooney and Anderson, 2014). In other words, glossier surfaces tend to be perceived as bumpier than diffuse surfaces.

Another surface property that influences perceived shape is the refractive nature of transparent objects. Images of thick transparent objects have complex structure attributed to their refractive power, shape, and material composition (Fleming et al., 2011b; Schlüter and Faul, 2014). It is also complex because natural transparent objects tend to have specular reflections on their surfaces. How do the refractive and reflective properties of transparent surfaces influence the perception of their 3D shape?

Although perceptual judgments of transparency loosely correspond to their refractive index (RI) (Fleming et al., 2011b), human observers are not able to accurately estimate the RI of transparent objects. The researchers proposed that perception of transparency was estimated based on the background distortion seen through transparent objects (Fleming et al., 2011b; Fleming, 2014; Todd and Norman, 2019). Another study proposed that background distortions alone are not sufficient for perceiving RI because they depend on both the shape and distance of the object from the background (Schlüter and Faul, 2014). Rather than observers matching internal experiences of refractivity, these researchers found that observers tended to match surfaces directly based on similarity in image cues: specular reflections and the distortion.

Further studies have used gauge figure tasks to estimate variations in perceived surface slant (i.e., surface curvature) and found that the 3D shape of objects with semi-opaque reflectance properties tends to be perceptually underestimated (Chowdhury et al., 2017; Schlüter and Faul, 2019). These interactions between perceived shape and material properties suggest that the perception of both shape and materials depends on similar sources of image-based information. Previously, I systematically varied the simulated material composition of objects from refractive to reflective, with different amounts of specular reflectance. I found that the thickness of objects with specular reflectance tends to be perceptually overestimated, and those of transparent objects were perceptually underestimated. I also found that the objects with 50% specular and 50% transparent components were perceived to have similar thickness to that of 100% specular surfaces as demonstrated in Figure 3.1 (Ohara et al., 2020). These results indicate that the specular component can dominate in the perception of 3D shape. This finding raises questions about what specular-refraction blend ratio would best mix these components to induce veridical perception of object thickness, and how perceived thickness alters as a function of the ratio of these two components. To address this question, I investigated thickness perception of objects that have different ratios of specular and refractive components. I also explored what image cues could determine this thickness perception.

## 3.2. Methods

### 3.2.1. Participants

Eight adult observers participated in an initial main experiment and nine observers participated in a follow-up experiment. All of whom had normal or corrected-to-normal vision. The participants ranged in age from 23 to 27 years. All participants were naïve to the purposes of this experiment. Informed consent was obtained from all participants. Procedures were approved by the Toyohashi University of Technology ethics committee. All research was performed in accordance with the relevant guidelines and regulations.

### 3.2.2. Stimuli

Figure 3.1 shows the objects used in this experiment. The shape of all samples and references was a sphere. The reason why I used only spherical shapes was because spheres were previously found to induce highly reproducible effects, compared with bumpy shapes used in my previous report (Ohara et al., 2020). There were two object stimuli: a reference and test stimulus. The reference was always a matte surface and was wrapped with a uniform dot texture (Figure 3.1, left). The test surface had either refractive, specular, or a mix of these components. Both refractive and specular components were generated separately, and then

mixed by weighted sum of them. There were eight ratios of purely specular component (0% (purely refractive), 0.625%, 1.25%, 2.5%, 5%, 10%, 20%, 40%). Although rendering transparency in this way is not physically correct, it held constant the refractive index at a value of 1.51. If physically correct rendering was applied to the transparent object, then changing the specular ratio would also alter the simulated refractive index and generate refractive distortions. However, I did not want the results driven by refractive distortions, since the aim in this study was to understand the relationship between the reflective properties of an object's surface and perceived thickness. The potential effect of this rendering on perceptual outcomes is considered further in the Discussion.

The reason why I did not use the objects with more than 40% specular in my experiments because the experimental results for these objects can be predicted from my previous studies (Ohara et al., 2020). In my previous study, objects with 50% transparency and 50% specular reflectance were perceived as having similar thickness to the object with only specular reflectance. There might difference between the specular ratio of 40% (max ratio of my current experiment) to 50% (ratio used in previous experiment), but the difference could be small.

All the stimuli were rendered using the open-source rendering package Blender 3D (Ver. 2.78, https://www.blender.org/). The 3D geometry was created in Blender 3D by taking an initial Ico Sphere with 20,480 triangle faces, 10,242 vertices (i.e., subdivisions = 6). This object's diameter was 1 Blender Units (BU, corresponding display size: 4.7 deg). All the stimuli were rendered with Cycles Render in Blender 3D. Cycles Render is a physically based ray tracing render engine designed for high-quality lighting simulation and animation.

The purely refractive component was simulated using a Refraction BSDF shader with zero roughness and applying Fresnel equations using the Mix shader. The Fresnel shader reproduces changes in refraction intensity that depend on the angle of the incident light. The RI used for generating refractive image was 1.51, which corresponded to crown glass. The purely specular component was generated by a Glossy BSDF shader with zero roughness and without Fresnel shading. Figure S3 shows the Blender node setup of this surface material.

I rendered images with limited linear tone mapping; the intensity of the specular highlights was limited by setting the exposure and any values exceeding the dynamic range of my standard RGB rendering were set to a maximum of 255. The monitor's calibrated gamma for displaying these images was 2.2.

I used six light probes including four indoor environments (Cathedral, Closed Bar, Dining, Grace) and two outdoor environments (Morning, Mountain) for rendering (http://gl.ict.usc.edu/Data/HighResProbes/ and http://illuminatedtools.com/freeprobes/). The right column in Figure 3.1 shows pure reflective specular objects embedded in each of these light fields. The relative position of camera and light probes was consistent through the study. The camera position was fixed to 10 BU away from the 3D object's center. The light probe images were used as environment maps projected on a sphere of infinite radius in order to illuminate the scene. This rendering setup was used to create movies that were shown to observers, as explained further below in the Procedure section. In these movies, the sphere sinusoidally oscillated along the horizontal axis at 0.5 Hz (amplitude = 2 BU, corresponding display size: 9.4 deg) which started from the center and moved rightwards. All the movie sequences were rendered using a custom Python script executed in the Blender 3D environment. All movies were rendered at 60 fps.

In the follow-up experiment, I examined the effect of 3D shape on perceived thickness. I used three different mesh geometries to assess the role of 3D shape (sphere, torus, bumpy; see Figure 3.3). The sphere was same as used the main experiment. The torus was made of an isometric tube whose diameter was 0.2 BU, and the distance from the center of the tube to the center of the torus was 0.4 BU. The angle of the torus was tangential to the camera, thus the total width of the Torus was 1 BU. This setting is a preset geometry of Blender 3D (Add > Mesh > Tours; Major segment = 200, Sub segment = 100, with 1,960,000 triangle faces, 980,000 vertices, subdivisions = 6). The bumpy geometry was the same as the shape used in my previous study (Ohara et al., 2020). In this experiment, the reference matte stimuli had uniform texture instead of the dotted texture, because it was not feasible applying dot textures to the torus and bumpy shapes. There were four specular ratios of (0%, 1%, 5%, 40%). There were three light probes (Morning, Cathedral, and Dining).

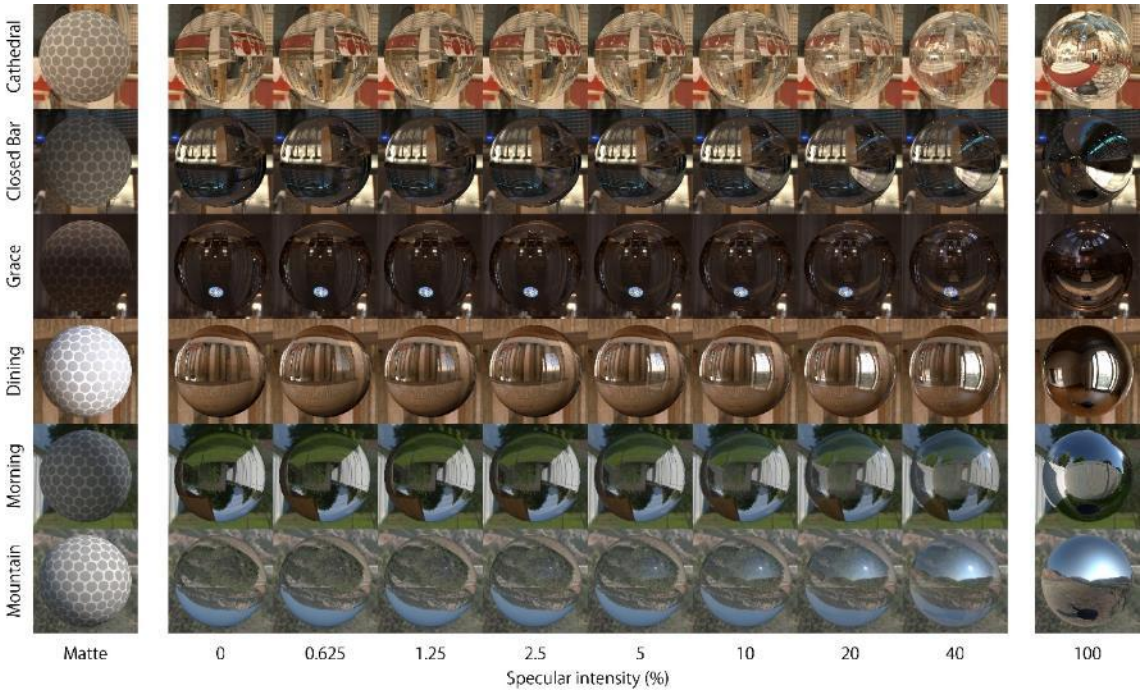


Figure 3.1: Appearance of stimuli. Matte and Test object (specular intensity: 0 - 40%) were used in the experiment in six light probes. The 100% specular surface was not used in the experiment.

### 3.2.3. Procedure

Environment and software used in the below experiment were the same as in the chapter 2. Two stimulus movies were shown separated horizontally. One of the stimuli was always the matte object, and the other was the test (supplementary movie 1). Position of the reference and test were randomized. Each stimulus size was 17 × 17 cm, 21.4 × 21.4 deg, 626 × 626 pixels including the object and background of the light fields, and area other than the stimulus movie was mid-gray (red = green = blue = 128). Observers were given a minute at the start of the experiment to practice a small number of randomly presented trials, before moving on to the formal testing session. The observers saw the stimuli with both eyes open.

It is known that the thickness of matte objects tends to be perceptually underestimated compared to ground truth under a single light source (Mooney and Anderson, 2014). However, thickness perception for diffusely reflecting objects may be more accurate, especially under complex light sources (Wilder et al., 2019). Thus, I reasoned matte objects should be an appropriate reference in complex illumination environments.

After watching the movies, observers were asked to choose which of the 3D objects appeared more elongated (like a rugby ball) in depth using the corresponding arrow key on the standard keyboard. No feedback on their response accuracy was provided. The movie continued to loop seamlessly until the observer responded. There was no time limit for the observer to respond. After pushing the response key, the next movie commenced playing immediately. Order of stimuli were randomized for the entire block of 54 conditions ((1 control + 8 specular ratio) × 6 light fields). In the control condition, both sides are matte object of same light probe. Observers performed 15 repeats for each stimulus condition.

Procedures used in the separate experiment were the same as in the main experiment, except for the number of the stimuli ((1 control + 4 specular ratio) × 3 light fields × 15 repetitions).

### 3.2.4. Statistical analysis

The observer's responses were analyzed using a generalized liner model (GLM). All statistical tests were performed using MATLAB (R2020b, Mathworks). The *fitglm* function with the link function for binomial distributions was used to perform GLM analyses. The *coeftest* function was used to calculate the effect of the specular ratio, light probes (in the main experiment), and object shape (in the follow-up experiment).

## 3.3. Results

Perceived thickness of the test objects relative to matte objects are shown in Figure 3.2. Observed probability increased overall as the specular ratio increased ($\chi^2 = 933$, df = 7, $p < 0.001$, GLM). This pattern in the data was consistent even when the analysis was performed for each light probes separately for at least 5 probes (Closed Bar: $\chi^2 = 32.4$, df = 2, $p < 0.001$, Grace: $\chi^2 = 18.4$, df = 2, $p < 0.001$, Dining: $\chi^2 = 11.7$, df = 2, $p < 0.001$, Morning: $\chi^2 = 102$, df = 2, $p < 0.001$, Mountain: $\chi^2 = 52.8$, df = 2, $p < 0.001$, GLM). It is important to note that the mean probability estimate across all specular ratios were different ($p < 0.001$, GLM). Across all light probes, the test object simulated with a 40% specular component was perceived thicker than the matte object. In three of six light probes, the Test object of 0% specular component was perceived flatter than the matte object. Hence, the probability estimate of perceived thickness did not increase linearly, but increased sharply around 0-0.05 of specular ratio.

The effects of different geometric 3D shapes on perceived thickness are shown in Figure 4. Observed response probability increased overall as the specular ratio increased for

all three shapes ($\chi^2$ = 152, df = 4, p < 0.001, GLM). This pattern in the response data was consistent even when the analysis was performed for each object shape (Sphere: $\chi^2$ = 62, df = 2, p < 0.001, Torus: $\chi^2$ = 5.04, df = 2, p = 0.02, Bumpy: $\chi^2$ = 16.4, df = 2, p < 0.001, GLM). Consistent with the main experiment, there were significant effects of different light probes on perceived thickness (p < 0.001, GLM). In summary, this follow-up experiment showed that perceived thickness increased with increasing specular ratio for all 3D shapes, and the increase was prominent around the 0-0.1 specular ratio. However, the torus induced rather consistent perceived thickness judgments irrespective of the specular ratio.

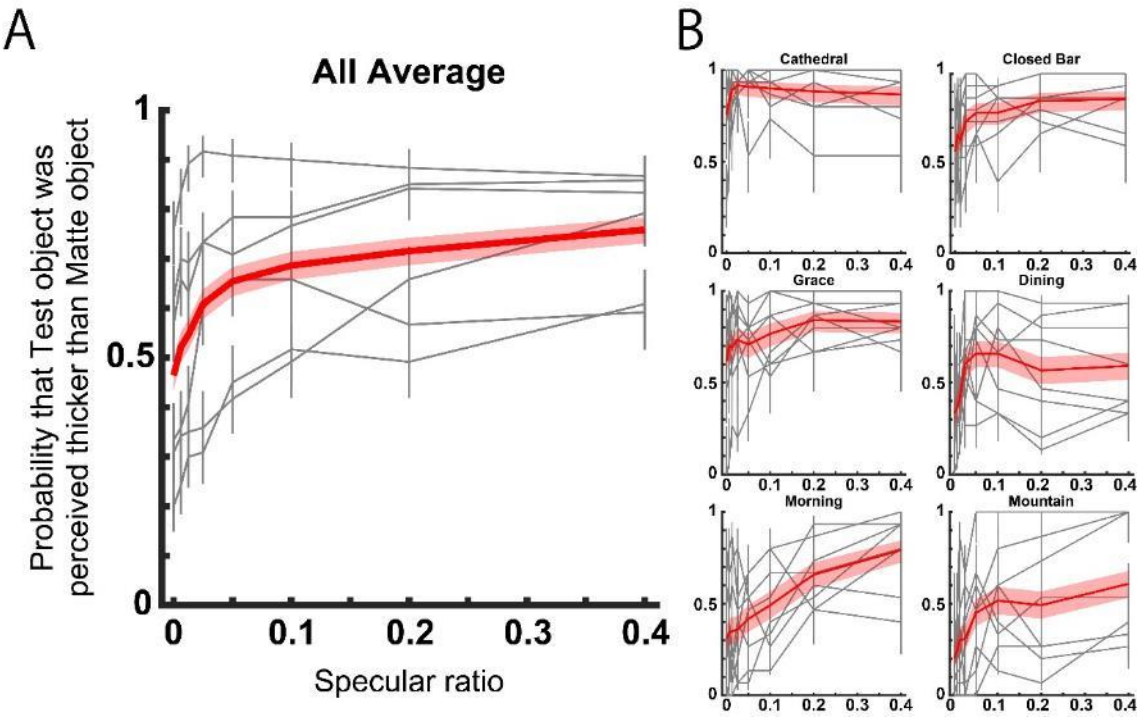


Figure 3.2: Perceived thickness for different light probe. (A) Plots show mean probability that the test object with each specular ratio was perceived thicker than the Matte reference object. The red line shows the average of all light probes and observers. Gray lines show the result by each light probe (shown in B as a red line). The red band and gray error bar show the 95% confidence interval. (B) Results shown separately for different light probes. The red line shows the average of all observers. Gray lines show the result of each observer. The red band and gray error bar show the 95% confidential interval.

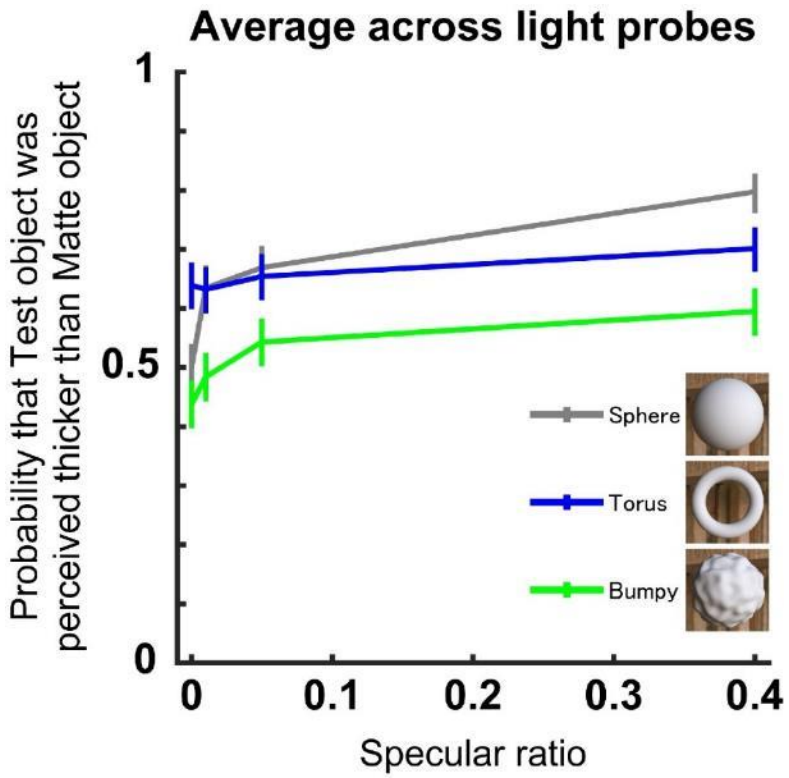


Figure 3.3: Perceived thickness for different 3D geometry of the object. Format is same as in Figure 3.2. Each line denotes a different 3D geometry, and the averages were computed across the three light probes and observers (n = 9). Inset shows the appearance of the three matte shapes illuminated using the Dining light probe.

### 3.3.1. Point of subjective equality (PSE)

In the main experiment, the test objects that generate 0.5 probability would be perceived to have the true thickness, assuming the observers perceived the true thickness of the matte object. On average, specular ratio of 0.049 induced true thickness perception. Hereafter, we use point of subjective equality (PSE) to denote the specular ratio that induces a 0.5 probability estimate of perceived thickness. For three of the six light probes, the PSE could be determined, and they ranged between 0.01 to 0.34 (Dining: 0.01-0.02, Morning: 0.05-0.15, Mountain: 0.05-0.34). The PSE was not determined in the other light probes, as the observed probability was larger than 0.5 at the 0 specular ratio. Thus, the specular ratio at the PSE could not be large. Those ratios were low suggesting that a small specular component would be enough for unbiased thickness perception. However, there remains a possibility that the effect of the reference stimulus (matte objects) may generate a percept that is different to veridical. This is further compounded by the possibility that the perceived shape of matte

objects may also depend on the light probe used. Thus, another index would be useful to determine the critical point of subjective equality in thickness between specular and refractive objects.

### 3.3.2. Midpoint

Increasing specular ratio from 0.0 to 0.4 generally increased the probability of perceiving an object as having greater thickness in depth. Which specular ratio generates the mean probability between them? The observed probability estimates increased steeply around the specular ratio from 0.00 to 0.05, but then increased more gradually up to the 0.40 mark. We calculated the specular ratio that induces mean probability in response to the 0% and 40% specular ratios. The midpoint was found to range between 0.02 and 0.2 (Cathedral: 0.02-0.025, Closed Bar: 0.02-0.05, Grace: 0.02-0.145, Dining: 0.02-0.03, Morning: 0.12-0.2, Mountain: 0.024-0.06). For the objects viewed in the three light fields where the PSE could be determined, these two points ranged between 0.01 and 0.34, smaller than the balanced (0.5) specular ratio. The differences in estimated midpoint suggest that different light fields have profound effects on relative judgments of 3D shape when observers compare transparent objects varying in sheen against completely opaque matte objects in the same illumination conditions.

## 3.4. Discussion

### 3.4.1. Summary

The experimental results showed that perceived thickness increased as a function of specular ratio – the proportion of the specular component that is combined with the refractive distortion field. In particular, the perceived thickness of objects increased markedly around the specular ratio range of 0% to 10%. Perceived thickness equivalent to the matte object was observed at less than 3.4% of the specular ratio. These results are consistent with my previous finding in which the specular objects are perceived as thicker than transparent objects without specular highlights, and the objects with specular highlights and transparency (1:1) are perceived similarly to specular objects (chapter 2). Results of the current study indicate that thickness perception changes markedly with very small percentages of specular reflection introduced into the image.

The follow-up experiment showed that perceived thickness increased as a function of specular ratio for all 3D shapes, although the magnitude of this effect varied across the

different 3D shapes used. Specifically, I was able to reproduce my finding that perceived thickness increases as a function of specular ratio for the bumpy object, but not for the torus. The reason why the tours shape did not produce similar results to the other shapes may be that the local surface orientation of tours is constant in the direction of its circumference and optically very narrow along its radius in the image. Thus, there was limited spatial variation in the local orientation cues available for the observer to use to form their thickness judgments. This was not the case for the doubly curved spherical smooth and bumpy objects, presumably due to the rich diversity in local shading cues available.

### 3.4.2. Why does perceived thickness increase sharply at low specular ratios?

Perceived thickness was most steeply increased around the 0% to 10% specular ratio. One possible explanation for this observation is that human observers are more sensitive to the addition of image features around the point of subjective equality to the matte reference object. Indeed, the observers' response most steeply increased around the point where the 50% probability response was observed, although there were large individual differences and the apparent light-probe dependency. Here, image properties should be more salient around the lowest specular ratio of 0% (i.e., based on Weber's law). I calculated how the variance of local RMS contrast changes with specular ratio (Figure 3.4). This variance of local RMS contrast image cue is seen to overall vary with specular ratios in a similar pattern to observer responses. The variance of local RMS contrast was highly correlated to the estimates of perceived thickness probabilities ($r = 0.79$, $p < 0.001$). This finding suggests human observers are sensitive to perceiving the shape of natural transparent objects with no specular reflections, or they can also perceive 3D shape in the 100% specular objects. This possibility is discussed in the general discussion.

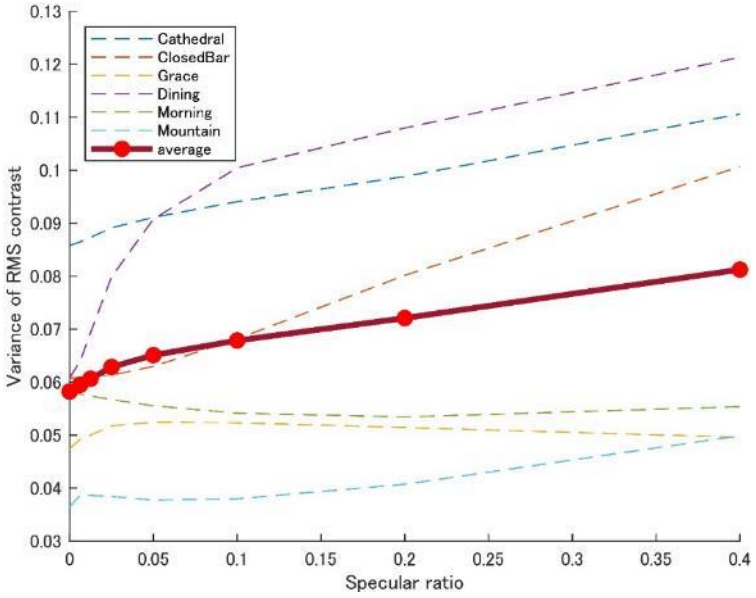


Figure 3.4: Variance of local RMS contrast by specular ratio. Plots show the mean variance in RMS contrast of Test objects in all six light probes as a function of specular ratio. The size of the region for calculating the variance of local RMS contrast was the same as used in Figure 3.4.

### 3.4.3. Physical validity of correct and accurate thickness perception

The test objects with specular ratios ranging between 0.01 and 0.34 were perceived as having similar thickness to the matte-textured 3D models' thickness. What visual cue might best help explain this result? There are several possible reasons that I explore below.

First, most ordinary objects have < 5% specular reflectance. For example, crown glass has 4.2% specular reflectance, and a ice has 2% in the air (Polyanskiy, 2008). It is possible that the participants were ecologically familiar with transparent objects through daily life learning and interaction. They would have been able to correctly estimate the thickness of the test stimulus when its reflectance was thus in the 3% to 5% range. They were also sensitive to the addition of contrast variations generated by the addition of small reflectance levels, thus the observed psychometric function was steep around these specular ratios.

Secondly, some artifacts may serve as cues because I used physically less rigorous rendering for transparent objects. In the rendering, I used a specific refractive index (1.51) to simulate transparent objects irrespective of the specular ratio. The image based on a specific refractive index (1.51) is perceived equivalent to the matte surface when the specular ratio is

4.3%, but when the reflectance deviates from this value, the image might look unnatural. Because it is known that reflectance (R) of an object is uniquely determined by the refractive index (n) (Hecht, 2002).

$$R = \left(\frac{1-n}{1+n}\right)^2$$

From the equation, the transparent object which has 1.51 refractive index reflects 4.3% of light when the incident light comes from the normal direction. However, RI=1.3 generates 1.7% reflection, and RI=2.0 generates 11% reflection. According to this view, the observer was able to estimate the correct thickness of the test stimulus around 4.3% of the specular ratio based on the transparent image with 1.51 RI. However, this possibility is unlikely because one study has shown that observers are unable to estimate the refractive index accurately (Fleming et al., 2011b). Nevertheless, observers may be familiar with the natural RI of common substances like water and glass. Thus, familiarity with certain RI indicates the potential involvement in familiarity of certain image cues.

## 4. Image cues explaining thickness perception

The experimental data have shown that the surface properties of objects affect the perception of their shape. What image cues produced by the interaction of the light field with different material surfaces evoke different perception of shape? Across the models I tested, a regional variation in local root-mean-square (RMS) contrast of the image was shown to provide good prediction of perceived depth of the objects. In this chapter, I explain how this model was introduced and examine the applicability to the observed data.

### 4.1. The variance of local RMS contrast model

In a recent study, Choudhury et al. assessed whether conventional shape from shading models for matter opaque objects might extend to translucent (i.e., non-opaque) objects (Chowdhury et al., 2017). They found that surfaces were judged as bumpier in 3D shape when generating local variations in image luminance over the same finite image space, compared with smoother surfaces. This finding revealed that generic computations of image contrast could be used to infer shape from shading across objects varying in opacity.

Although completely refractive transparent objects lack this diffuse shading, it is possible that similar computations of local image contrast could be used to also infer their 3D shape. Fleming et al. showed that highly curved regions of specular surfaces generate higher spatial frequency distributions in the contrast variations of the reflected light field (Fleming et al., 2004). Alternatively, flatter surface regions reduce this spatial frequency, which would have the effect of reducing local contrast energy at local surface regions. Hence, in a similar way to matte objects, I expect that local contrast variations in image structure will still be diagnostic of local surface curvature and thus the thickness of objects in depth. Indeed, previous studies have shown that changes in the distribution of environmental edge contours are informative of an object's material composition and likely also 3D shape (Kawabe et al., 2015; Dövencioğlu et al., 2018). Based on these evidence, variations in local image contrast may inform the perception of shape from distortions of the light field transmitted through the body of refractive objects. I explore the utility of computing local RMS contrast for these refractive materials.

Calculating the variance of local root-mean square (RMS) contrast corresponds to the activity of two hierarchical filters. First, local RMS contrast models the activity of the primary visual cortex, which responds to various types of spatial contrast and intensity (Hubel and Wiesel, 1962; Freeman et al., 2013; Rieger et al., 2013). The RMS contrast was preferred describing detectability of natural images (Bex and Makous, 2002; Pelli and Bex, 2013).

Second, the variance of local RMS contrast models cells found at higher levels of visual processing (Freeman et al., 2013). Here, I applied the same model to examine whether perceived object thickness in depth could be explained computationally. The RMS contrast of the stimulus images is computed by the following formula:

$$RMS\ contrast = \sqrt{\frac{1}{N}\sum_{n=1}^{N}|{x_n}^2|}$$

where x is pixel luminance, and N is number of pixels for analysis.

## 4.2. Image analysis (for Experiment 1 of chapter 2)

### 4.2.1. Apply the variance of local RMS contrast model

I computed local RMS contrast over finite image regions defined within 15×15 pixel (1.0× 1.0 deg) square tiles (Figure 4.1A, B). Then, I calculated the variance of RMS contrast over regions defined within 6×6 tiles (Figure 4.1C). Thus, each variance was computed over 90× 90 pixels (6.1×6.1 deg) of the stimulus image.

To assess the validity of my model, I computed the correlation coefficient between the variance of local RMS contrasts and perceived convexity (Figure 4.1D and E) using stimuli images and observers response in chapter 2. The data for perceived convexity used here were for the condition with static stimuli presented at the center of the display. The large green symbol in Figure 4.1D indicates the data from the smooth sphere (convexity = 1) in the Eucalyptus Grove light probe (Figure 4.1A-C). Correlation plots between the variance of RMS contrast of the region with highest correlation (denoted by red square in E) and perceived convexity. Figure 4E shows the distribution of the correlation coefficients (Spearman's R value) for each analyzed image area. Significant correlations were observed for the upper half of the image (denoted by white outline in Figure 4.1E, significant correlation, $p < .05$). Highest correlation was found for right side of the image ($R = 0.81$, red outline in Figure 4.1E). A similar conclusion was obtained for different region size for calculating RMS contrast and tile size for calculating the variance (Figure S2 in Supplemental Material). These results suggest that perceived convexity can be explained by variance of local RMS contrasts at different parts of the image.

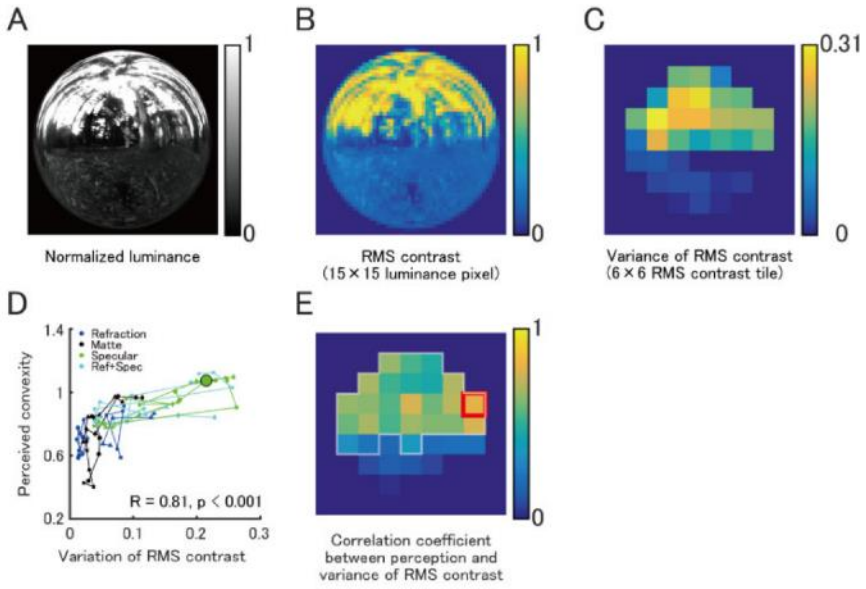


Figure 4.1: Correlation between local RMS contrast variability and perceived convexity. A: Normalized luminance image of an example stimulus. B: Local RMS contrasts over finite image regions defined within 15 × 15 pixels were computed. C: The variance of RMS contrast within the regions of 6 × 6 RMS contrast areas was computed. D: Correlation plots between the variance of RMS contrast of the region with highest correlation (denoted by red square in E) and perceived convexity. Color of symbols shows surface properties. Shape of symbol indicates the light probe and stimulus shape (circle: Grove–Smooth, diamond: Grove– Bumpy, square: St Peters–Smooth, triangle: St Peters–Bumpy). Symbols connected by lines indicate five levels of stimulus convexity (E). The Spearman's rank correlation coefficient was calculated separately for each variance of RMS contrast. White outlined areas showed significant correlation ($p < .05$). RMS = root-mean-square. geometry

### 4.2.2. Discussion

Variation in local RMS contrast around the upper half image region was shown to provide predictive leverage in estimating perceived surface convexity.

It is possible that the visual system may infer the shape of objects by variations in the compression gradients in these distortions. Indeed, the human visual system can estimate an object's surface curvature from the distortion of surface textures and can also estimate object shape from this curvature information (Fleming et al., 2004; Todd and Thaler, 2010). This relationship between perceived shape and the distortion field can even be used for devising computations for estimating the relative convexity of objects; however, these computations

do not reveal the magnitude of an object's true convexity (Sakai and Finkel, 1995). The degree of distortion of the refractive object's surface appearance also depends on the RI (Fleming et al., 2011b; Kawabe and Kogovšek, 2017). Thus, it may be difficult to estimate the magnitude of the convexity based on surface appearance.

Consistent with the view that the distortion field contributes to shape estimates, I found that variation in local RMS contrast of the surface could account for perceived convexity. I provided some computational evidence to suggest that observers might use this information within the upper portion of the image. It is possible that information concerning the shape of the bounding contour is also used to supplement the upper gradient information to experience shape across the entire region of the surface's image (Fleming et al., 2009).

## 4.3. Image analysis (for Experiment 2 in chapter 3)

### 4.3.1. Apply the variance of local RMS contrast model

I also applied the variance of local RMS contrast model to stimulus images and observers' responses in chapter 3. I computed local RMS contrast over finite image regions defined within $7 \times 7$ pixel square tiles of the luminance image (Figure 3.4A and B). Then, I calculated the variance of local RMS contrast over regions defined within $4 \times 4$ tiles (Figure 3.4C). Thus, each variance was computed over a $28 \times 28$ pixel region of the stimulus image. This procedure was repeated for all frames of each stimulus movie.

Figure 4.3 shows a correlation plot between the variance of local RMS contrasts and the average probability estimate of stimuli being selected as thicker for each light probe. The image regions which have highest positive correlation are designated separately for calculating the variance of local RMS contrast (tiles outlined in blue for each heatmap). The observed highest positive correlation coefficient (Spearman's Rho) was found to be significant ($p < .05$). Significant correlations were also observed in other regions of the image (white outline in each heatmap). The highly positive correlations were found in different regions of the surface image across the six light fields. Similar conclusions were found when different regional sizes were used for the calculation of local RMS contrast and the tile size for calculating the variance (Figure S4 in Supplemental Material). Correlation coefficients calculated for each subject separately showed a similar trend, with significant correlations for all light probes. The above mentioned analysis was performed for a certain frame (center) of the movie, but similar conclusions could be drawn for different stimulus object positions during lateral motion (Figure S5 in Supplemental Material). These results indicate thickness perception can be explained by the variance in values of local RMS contrasts, but the surface regions of importance appear to vary across light fields due to differences in the optical structure.

There are tiles that are highly positively correlated for each of the six light probes (Figure 4.3). The distribution of tiles with high correlation is similar to the distribution of tiles with high variance in the local RMS contrast of the 100% Specular image (Figure 4.4). This result suggests that the observer may have used the brighter image regions of the reflectance image as a cue to estimate object thickness. Indeed, Figure 4.5 shows the correlation coefficients between my model (Figure 4.3) and the 100% specular image's variance in local RMS contrast or mean luminance of the corresponding local neighborhood pixels of each stimulus separately for the six light probes. Generally, image regions of greater luminance and variation in local contrast generated correlations with psychophysical data that were overall stronger, suggesting the visual system may use these local image features to

identify critical regions for assessing an object's 3D shape.

The Grace and Cathedral light fields deviate from the pattern seen in the data for the remaining light fields. It is possible that in the case of the very dark Grace light field, image regions that exhibit greater variation in local RMS contrast and not just higher local luminance are used when assessing 3D shape. For the Cathedral light field, the pattern of psychophysical data was confined to a very tight range of very high probability estimates for perceived thickness, which may be attributed to the comparatively very low image contrast generated by the matte reference stimulus.

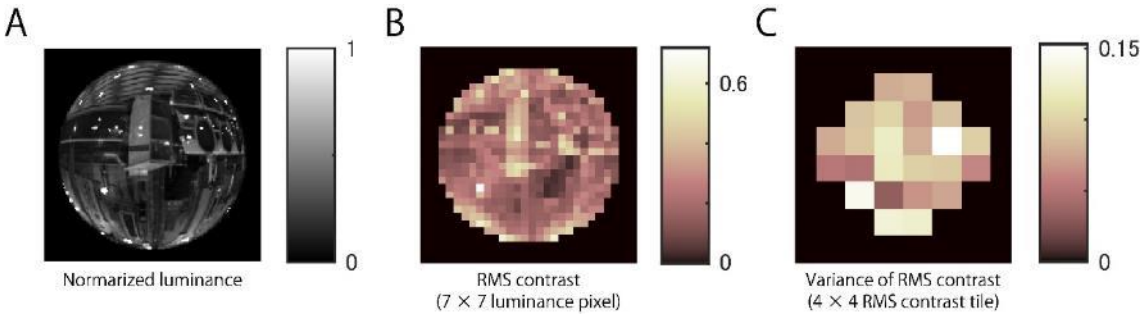


Figure 4.2: Local RMS contrast variability. (A) Normalized luminance image of an example stimulus. (B) Local RMS contrasts over finite image regions defined within 7×7 pixels were computed. (C) The variance of RMS contrast within the regions of 4×4 RMS contrast areas was computed. RMS: root-mean-square.

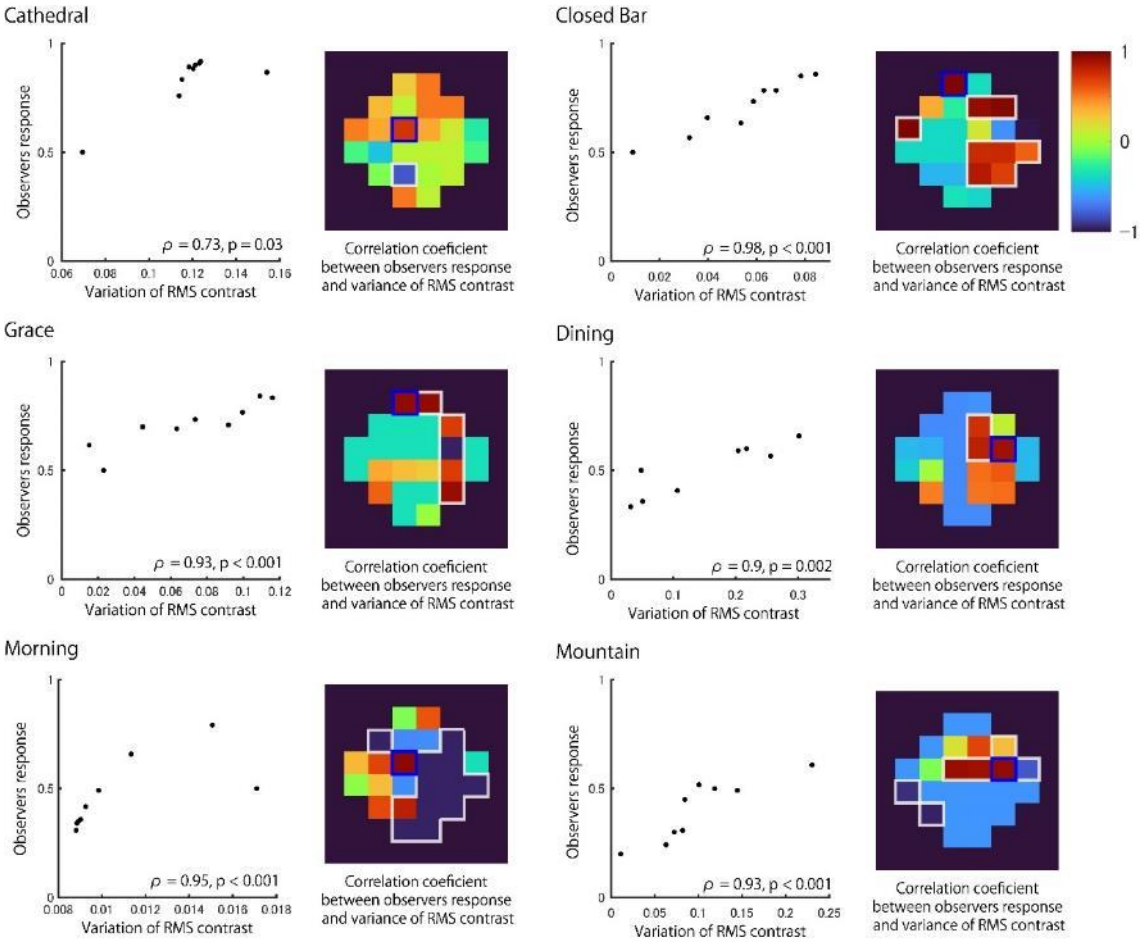


Figure 4.3: Correlation between local RMS contrast variability and observer response for each light probe. Correlation plots between the variance in local RMS contrast of the region with highest correlation (denoted by blue square in heatmap) and the observers' response in each light probe. Data includes the reference (matte) and corresponding response was assumed to 0.5. Heatmap show the Spearman's rank correlation coefficient was calculated separately for each region. The region with white outline shows significant correlation ($p < .05$).

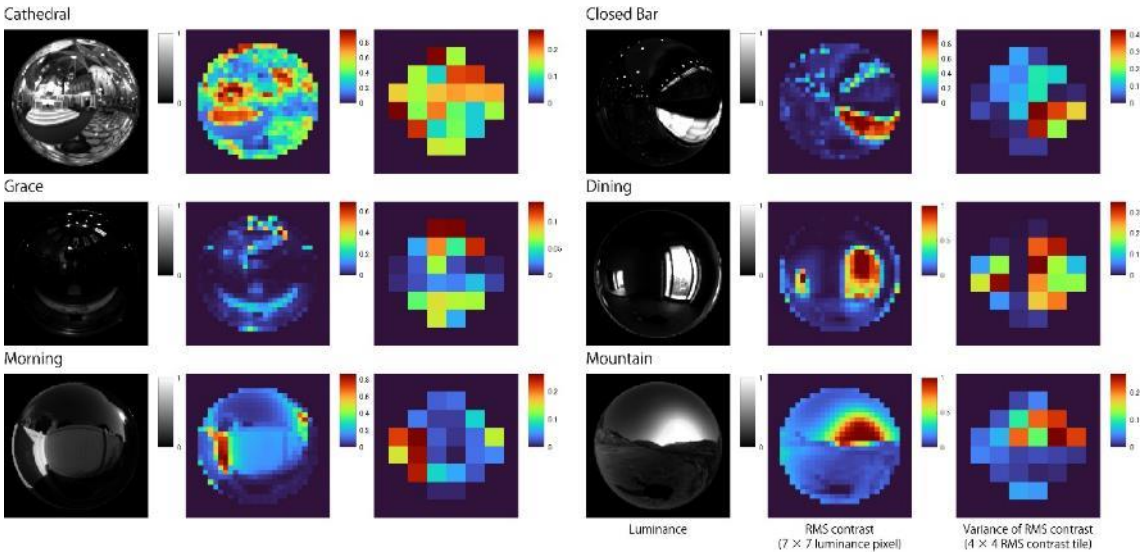


Figure 4.4: Heatmaps showing the variance in local RMS contrast for the 100% specular surface in each of the six light fields. Note that regions of local maxima for variations in RMS contrast generally coincide with brighter image regions.

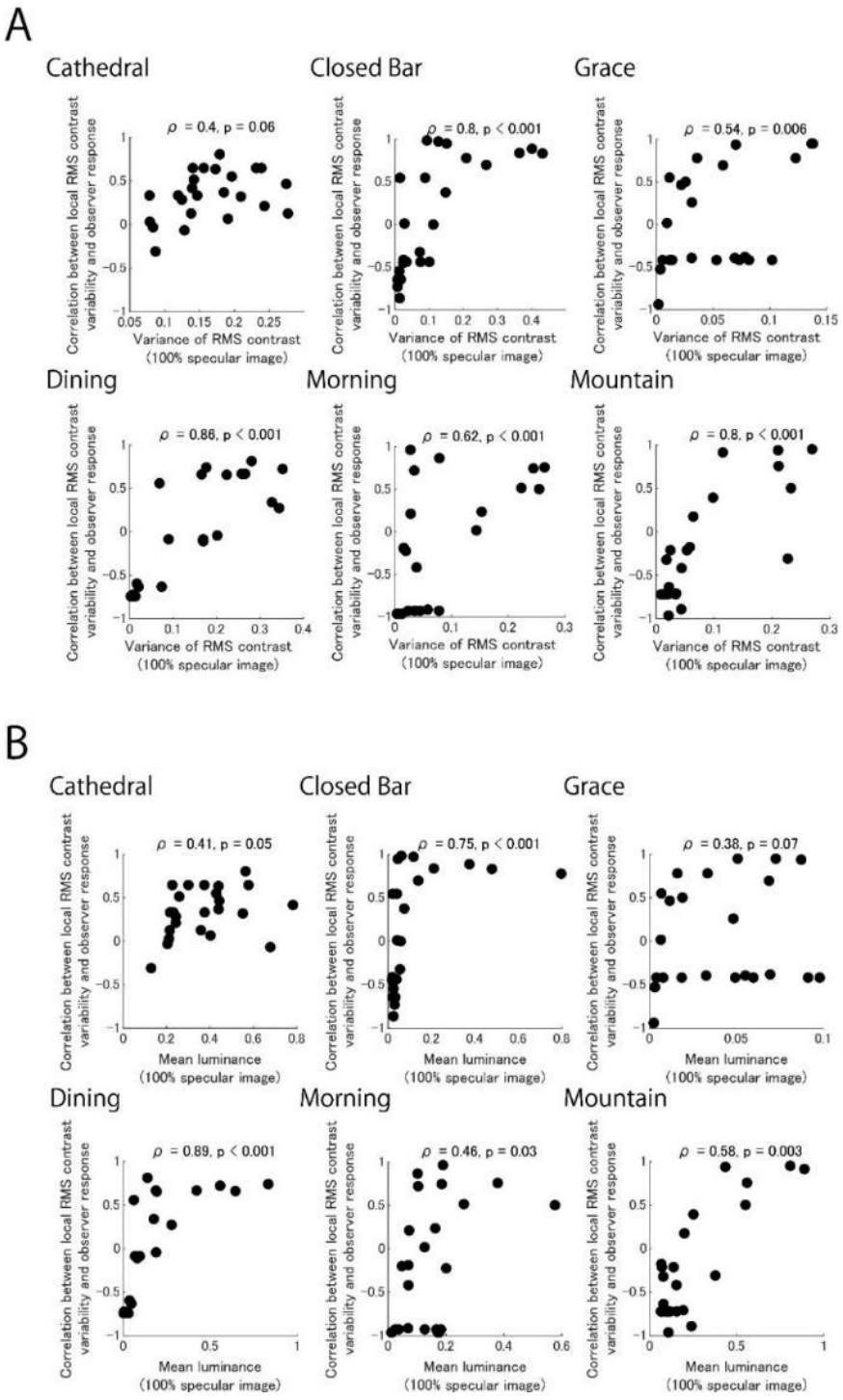


Figure 4.5: Black dots show each of the 24 correlation coefficients for my model in each pixel region of images shown in each image of Figure 4.3 plotted as a function of image parameters for the 100% specular image component (Figure 3.1Figure 3.1Figure 3.1). Separate panels show model performance for six light fields plotted against local variation in RMS contrast (A) and local image luminance (B).

### 4.3.2. Other models | Raw image statistics

Previous researchers have found a positive correlation between the perceived gloss and skewness of luminance histograms of images (Motoyoshi et al., 2007). Surface gloss has also been shown to increase perceived surface convexity (Mooney and Anderson, 2014). It is therefore possible that perceived surface convexity could be explained by the skewness of the luminance histogram of images.

If histogram skewness of stimulus images can account for perceived convexity, the luminance histogram of the purely refractive object's image should have lower skewness than all other surface materials. Contrary to this prediction, however, Figure 4.6 shows that such a trend was not observed. Image skewness decreased with increasing physical convexity. Moreover, these declines in skewness were different across the two light probes used. Figure 4.7 also shows that even perceived convexity does not show any relationship with image skewness. Contrary to the view that histogram skew predicts perceived convexity, I found that perceived convexity decreased with increasing image skewness, and the order of offset in traces plotted did not consistently adhere to the ordering of perceived convexities found in previous experiments across surface materials and light probes used.

Standard deviation of image, which also contributes to glossiness (Motoyoshi et al., 2007), had some similarity with perceived convexity. The purely refractive object had the lowest standard deviation and was perceived to have the lowest convexity across surface bumps and light probes (Figure 4.8, Figure 4.9). However, the purely matte surface had the greatest RMS contrast for the highest convexity levels in the St Peters Basilica light field. It would appear that any potential role of RMS contrast per se in estimating surface shape is limited.

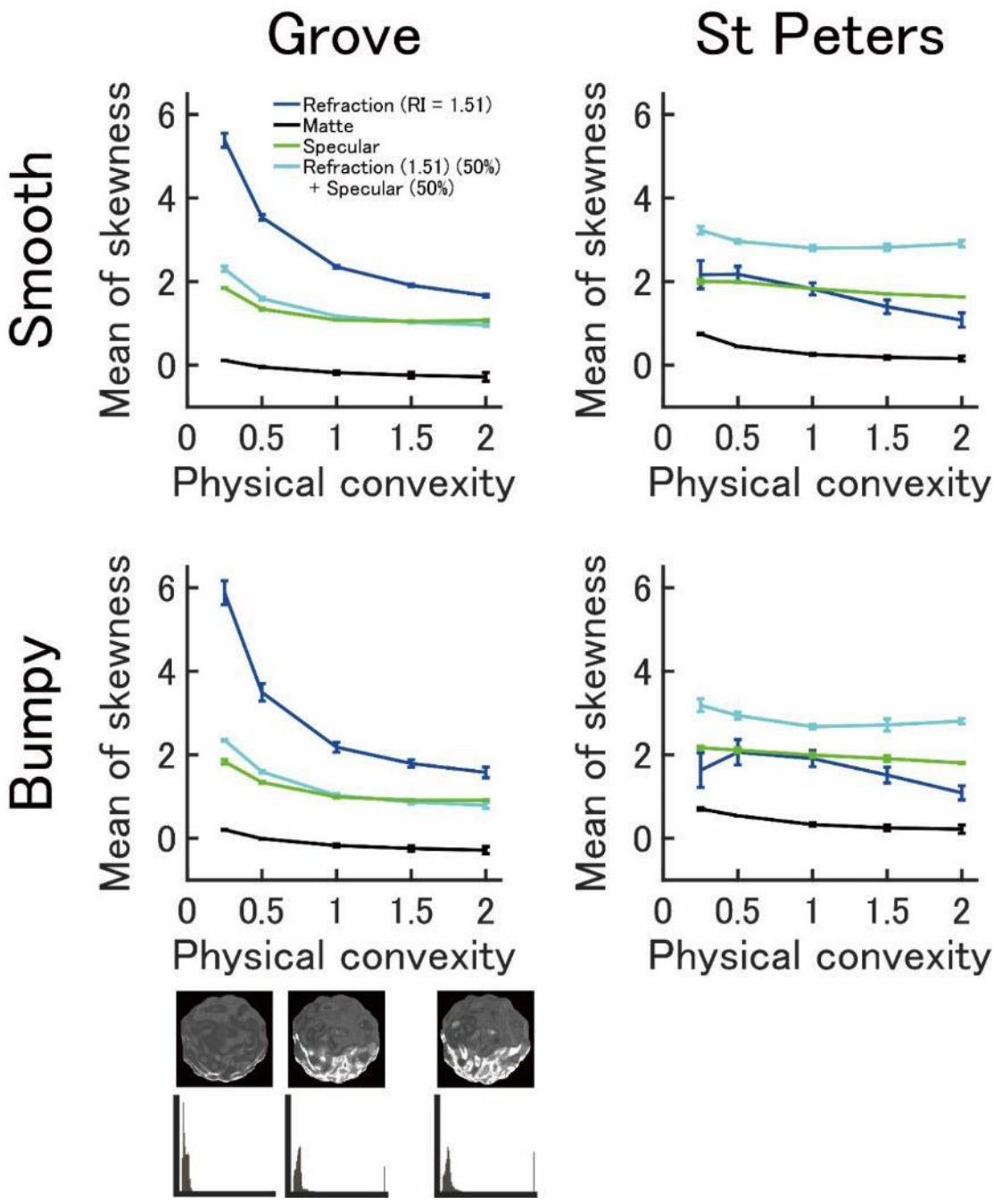


Figure 4.6: Skewness of image luminance histogram. Plots show mean skewness of luminance histograms as a function of physical convexity of objects with different simulated material properties. Only pixels of the object drawn in images were used in the calculation. Inset pictures and histograms indicate the appearance of images and the luminance histograms of bumpy purely refractive objects in Eucalyptus Grove. Convexities of 0.25, 1.0, and 2.0 are shown from left to right. The error bars show the standard deviations of the means of 60 frames.

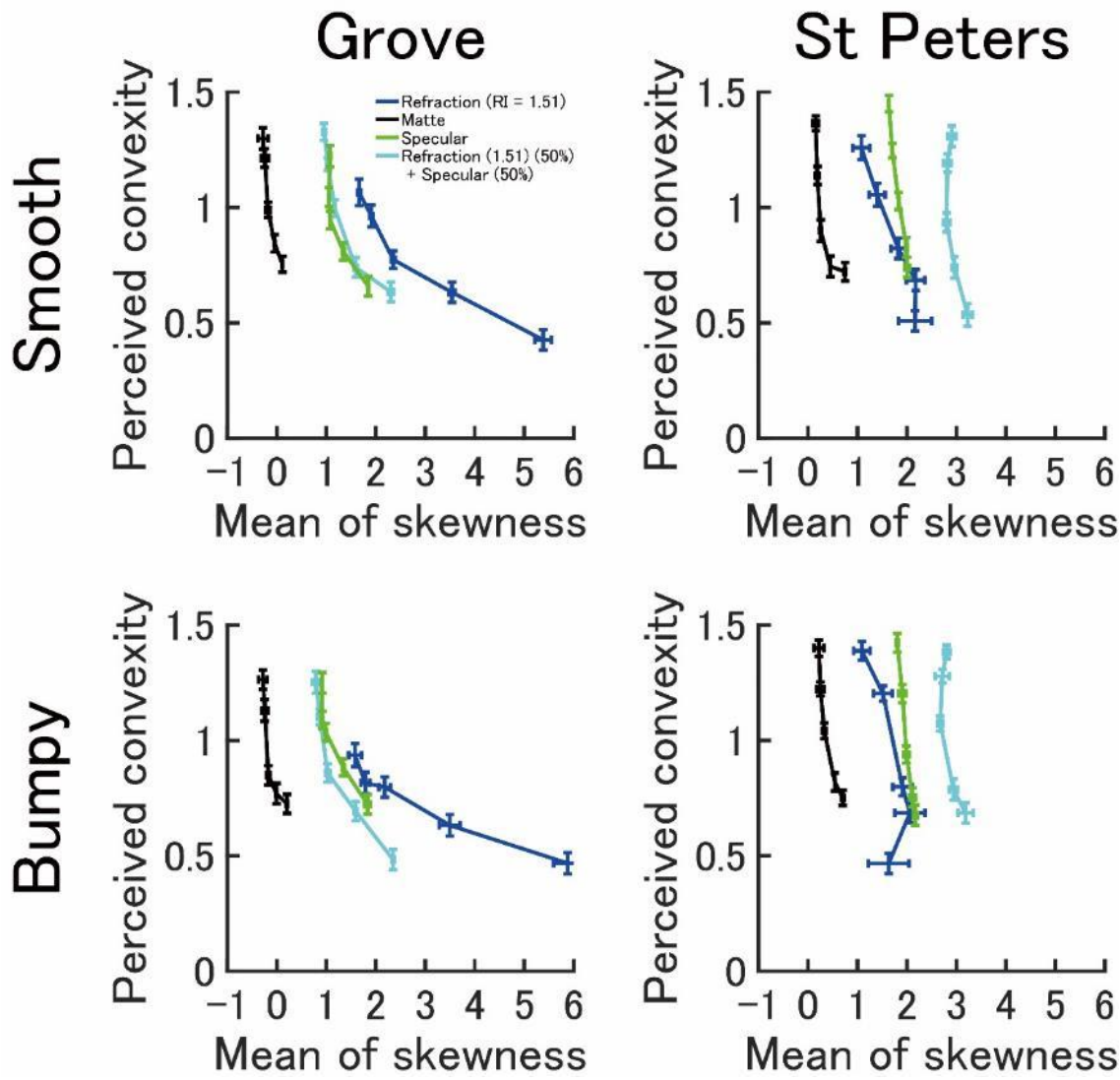


Figure 4.7: Skewness of image luminance histograms. Plots show perceived convexity as a function of mean skewness of the luminance histograms of objects with different simulated material properties. Only pixels within the object space were used in the calculation. Vertical error bars show the standard deviations of the means of 60 frames. Horizontal error bars show the standard errors of the means of all means of all observers.

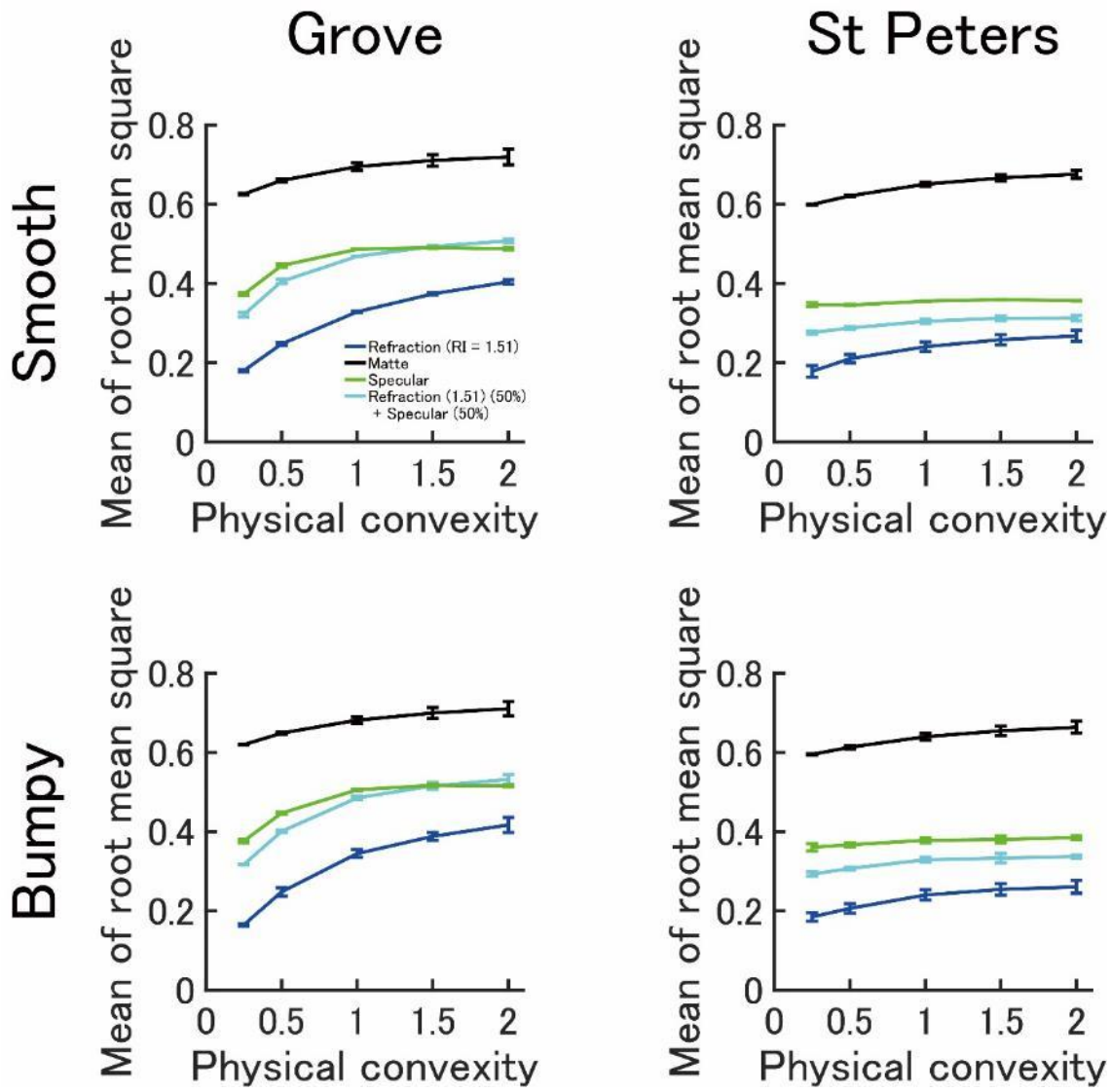


Figure 4.8: RMS contrast of image luminance histograms. Plots show the mean standard deviations of the luminance of objects as a function of the mean standard deviation of perceived convexity with different simulated material properties. Only pixels for the object regions were used in the calculation. The error bars show the standard deviations of the means of 60 frames.

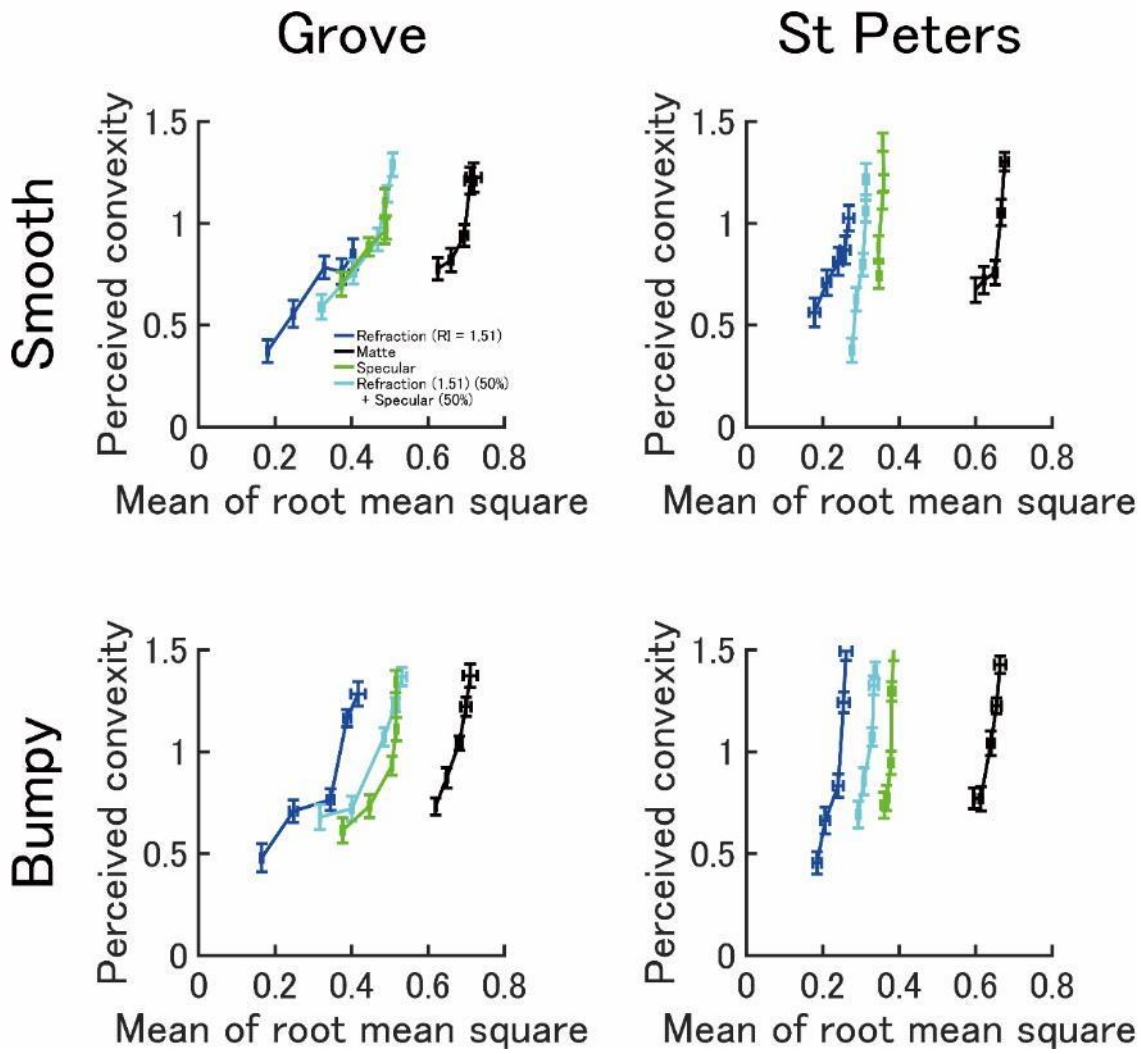


Figure 4.9: RMS contrast of image luminance histograms. Plots show perceived convexity as a function of RMS contrast for images of objects with different simulated material properties. Only pixels in object regions were used in the calculation. Vertical error bars show the standard deviations of the mean of 60 frames. Horizontal error bars show the standard errors of the means of the means of all observers.

### 4.3.3. Other models | Sub-band image statistics

Shading is critical for shape perception, and it is possible that shading might contribute to the estimated convexity of shape stimuli. Elongated objects tend to have high luminance contrast compared to flatter objects due to their steeper shading gradients (Ramachandran, 1988). These shading components would be expressed in lower-band power of the images. Here, I focused on the sub-band power of the stimuli used.

As in the previous analyses, color images were converted to gray scale, assuming sRGB standard. I applied band pass filters with low band (Differential gaussian filter, standard deviation = 32 – 64 px), middle band (8 – 16 px), and high band (2 – 4 px) characteristics to each frame of the grayscale stimulus movies. The images of the background were filled in black, and filters were applied to the object regions (Figure 4.10 bottom). The contrast of the sub-band images was then calculated for RMS contrast over the object region. If observers' estimation of convexity simply relies on RMS contrast in the lower sub-band irrespective of surface material, RMS contrast should account for changes in convexity (Figure 2.2). As expected, RMS contrast gradually increased with increasing physical convexity, especially in low-band images. However, the arrangement of curves cannot account for my psychophysical data from experiments (Figure 4.10 top). For example, the RMS contrast of matte objects was overall larger than the other surface materials, including the specular materials.

The RMS contrast of middle bands had relatively good correlation with perceived convexity, especially in low convexity stimuli. The RMS contrast of the refractive object tended to be lower than that of other surface materials. Objects with greater convexity had similar RMS contrast. The higher band generated RMS contrast curves that did not reflect the slopes of the psychophysical data. Correlation coefficients indicate that the RMS contrast of middle bands maximally explain psychophysical data irrespective of surface quality of the stimuli

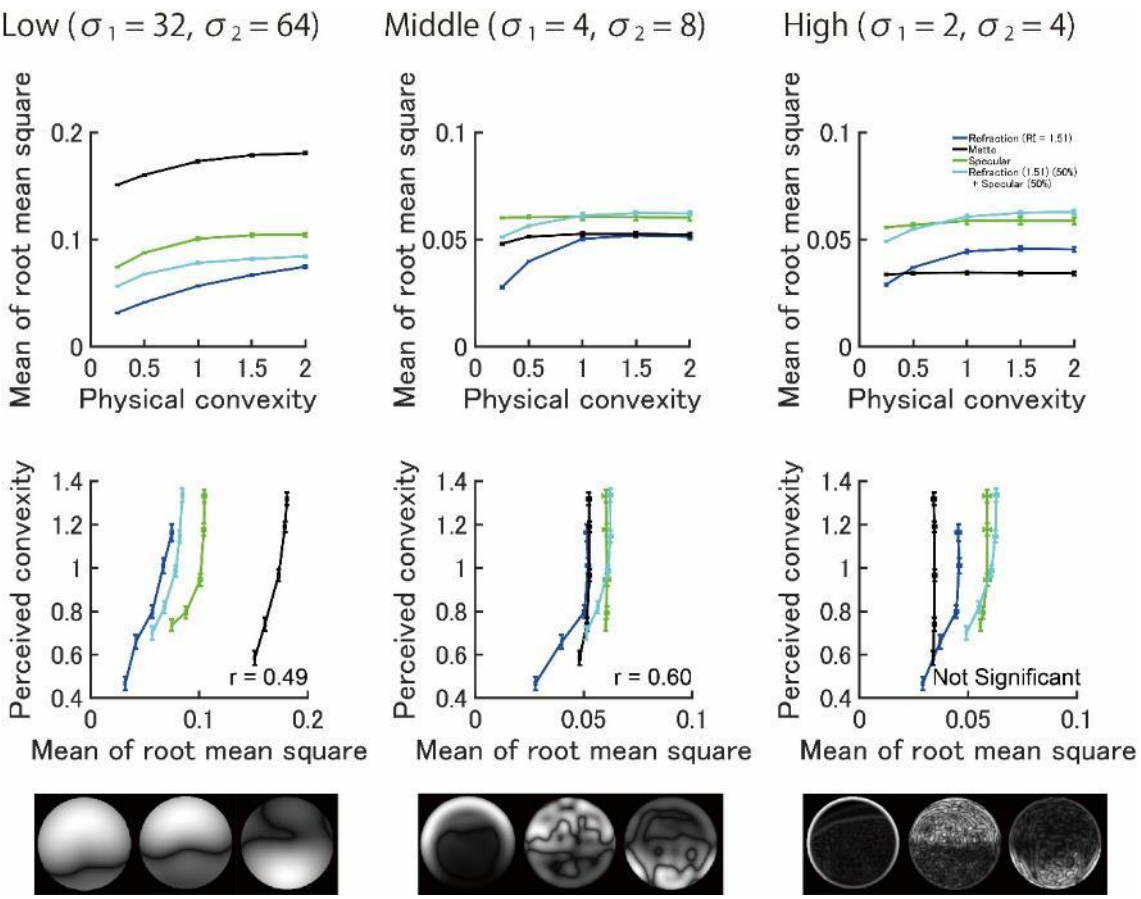


Figure 4.10: Sub-band power of stimuli images. Top row: the error bars show the standard deviations of the means of 60 frames. Bottom row: plots show the perceived convexity of objects as a function of the root mean square of luminance distribution of stimuli images with different simulated material properties. Stimulus images were processed with different size Gaussian filters (low, left; middle, center; high, right). Inset pictures are the filtered images of the smooth object in the Eucalyptus Grove light field (matte, specular, and refraction, shown from left to right). The vertical error bars show the standard error of the means of all observers. The horizontal error bars show the standard error of the means of 60 frames. R values were shown in bottom figure indicate significant ($p < .05$) correlation coefficient.

## 4.4. Discussion

### 4.4.1. Possibility of the variance of local RMS contrast as a depth cue

The analysis shown above have confirmed that the variance of RMS contrast most accurately explained the perceived thickness of the objects. Perceived thickness of spherical object with specular component increased overall as specular ratio increased. Then highly positive correlation was observed between specular ratio and variance of RMS contrast. One limitation

is that the almost all objects in my study have spherical shape under the limited number of light probes. In this section I show that for the objects other than spherical shape under hundreds of light probes, the variance of RMS contrast is applicable as same as the sphere. By showing that the variance of RMS contrast varied depending on the thickness of the objects and the percentage of specular reflection on surface.

Five convexities (depth level) of sphere and bumpy object were calculated variance of RMS contrast (which same as Figure 2.1A). I used one hundred eight light probes (2 from chapter 2 + 6 from chapter 3 + 100 from Poly Haven (https://polyhaven.com/hdris)). A light probe was rendered at four different azimuth angles (0, 45, 90, 135 degs). The surface material is same as the Test object in experiment. There were six specular ratios (0, 0.01, 0.05, 0.1, 0.4, 1) in this analysis. Figure 4.11 shows the average of variance of local RMS contrast as a function of object convexity by specular ratio. I computed local RMS contrast over finite image regions defined within 7×7 pixel square tiles of luminance image. Then, I calculated the variance of local RMS contrast over regions defined within 4×4 tiles and averaged all tiles.

For all specular ratio, average of variance of local RMS contrast increased with convexity (three-way ANOVA, main effect of convexity, $F(4, 619233) = 3764.55$, $p < 0.001$, partial $\eta^2 = 0.02$). This trend suggests that variance of RMS contrast could be the depth cue.

The variance of RMS contrast also changed with increase specular ratio (three-way ANOVA, main effect of specular ratio, $F(1, 619233) = 6977.24$, $p < 0.001$, partial $\eta^2 = 0.001$).This trend suggest that specular ratio contributes to the illusionary effect which perceptual depth of object increase with intensity of surface specular reflection.

The variance of RMS contrast increased with both specular ratio and convexity. This trend indicates that the variance of RMS contrast can be controlled by using these two physical factors. The thickness perception obtained by psychophysical experiments is explained by the variance of RMS contrast. Therefore, it is possible to control the thickness perception of an object by controlling the specular ratio of the material or convexity.

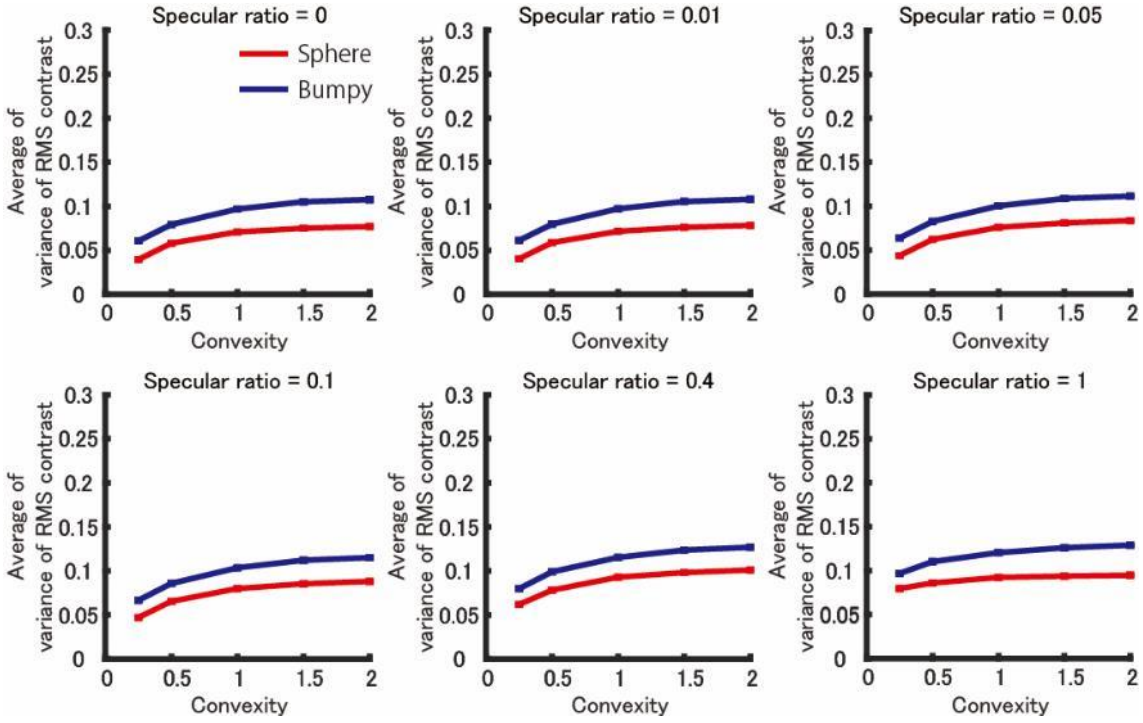


Figure 4.11: Average variance of local RMS contrast by specular ratio. Plots show the mean of average variance of RMS contrast of objects in all one hundred eight light probes as a function of object convexity. The red line shows result of sphere shape, and blue line shows result of bumpy shape. Error bars show standard error of mean.

### 4.4.2. Other model for thickness perception

Orientation map is a thickness perception model proposed in previous studies (Fleming et al., 2004; Shimokawa et al., 2019)(Fleming et al., 2004; Shimokawa et al., 2019). This model estimates the orientation of object surface normal in an image by calculating the local luminance gradient vectors in the x- and y-directions.

The advantage of the orientation map is that it can estimate the shape of the whole object. However, the orientation map is sensitive to changes in the luminance of the pixel of interest and its neighbors, so it does not correctly estimate the normals of overly distorted reflections when applied to transparent objects (Chen and Allison, 2013). The orientation map is probably effective only for opaque objects with diffuse or glossy reflections.

On the other hand, the advantage of the variance of local RMS contrast is that it can serve as a model of the subject's shape perception even for objects whose images are excessively distorted by two pooling operations (obtaining the RMS contrast and calculating

its variance). In addition, the variance of local RMS contrast is a model that can explain the subject's shape perception with less computational effort than the orientation map. However, it is poorer than the orientation map in that it does not have enough information to recover the shape of the entire object.

The variance of local RMS contrast model is an alternative thickness perception estimation model to the orientation map for objects with transparent properties. It can also be proposed as an effective model for objects with complex textures created by specular reflection.

### 4.4.3. The generality of variance of local RMS contrast model

I analyzed observers' responses based on variance of local RMS contrast in stimulus images including matte, specular, and transparent objects. The motivation for using variance of local RMS contrast came from previous work on the perceived shape from shading of translucent objects (Chowdhury et al., 2017). Indeed, other previous works have suggested that the visual system relies on common image features, irrespective of their material differences. For instance, humans appear to use common image features when perceiving the shape of matte and velvet objects (Wijntjes et al., 2012; Sawayama and Nishida, 2018). Some studies have attempted to devise generic models for the perceived shape of opaque objects (Fleming et al., 2004, 2011; Kunsberg and Zucker, 2021). However, neurophysiological research further supports the view that there are generic mechanisms of 3D shape recovery in the brain. A recent neuroimaging study has reported that there are V4 neurons selective to shape information irrespective of material differences (Srinath et al., 2021). Together, these studies indicate there exist potentially generic shape cues that are independent of an object's material properties. Although these cues may be context specific, one possible cue might be the variance of local RMS contrast proposed here, which was found to be applicable to the estimation of 3D shape of objects with different simulated material compositions.

# 5. General discussion

## 5.1. The effect of unnatural stimulus rendering

The upper row in Figure 5.1A shows physically more rigorous rendering of transparent objects with different levels of refractive index. Images in the middle and bottom rows show specular and refractive components of the image in the top row. These images showed that not only does the relative intensity of specular and refractive components vary, but also the transparent image deforms depending on the RI. In contrast, the stimulus images used in the experiments did not deform across specular ratios because I used a fixed RI (1.51) (Figure 5.1B). I only manipulated relative intensity of specular and refractive components to examine the effect of specular ratio.

The reason why I adopted this rendering approach is that I aimed to examine the relative contributions of the intensity of the specular reflection while keeping the deformation of the refractive image constant. Image distortion may affect thickness perception, nevertheless my simplification of the rendering manipulation reveals the importance of relative specular amplitude rather than the effect of image distortion per se. This approach is different from previous studies that examined the relationship between shape perception and refractive index estimated by changing the degree of distortion (and intensity of specular reflections) generated by manipulating refractive index (Fleming et al., 2011b; Kawabe and Kogovšek, 2017; Schlüter and Faul, 2019).

In Experiment 1 (Chapter 2) I found that the refractive component reduced thickness perception. In contrast, the reflective component enhances thickness perception (Nishida and Shinya, 1998; Mooney and Anderson, 2014). To understand the relative contribution of the specular and refractive components in Experiment 2, it was necessary to manipulate the specular ratio in combination with image structure attributed to other material properties like transparency.

The image processing required to compute variance in local RMS contrast involves calculations from luminance values directly obtained from the images with both reflective and refractive components combined, rather than calculating it based on the reflective and refractive images separately. I have already found that mixing the two images by 50% generates the same thickness perception as achieved by the specular image alone in Experiment 1, and since the two images are different, the variance of local RMS contrast will produce different outputs. It is still possible that observers may have estimated the object's thickness after first separating specular and transparent components, rather than directly

from the combined image.

The use of unnatural stimuli may have caused the subjects to perceive the spherical objects as bubbles instead of solid transparent objects, or non-rigid shape changes with the objects' movement (Kawabe et al., 2015; Dövencioğlu et al., 2018). Although I did not ask the observers to report their perceptual estimates of material class or rigidity in the experiment, none of the participants reported these distortions.

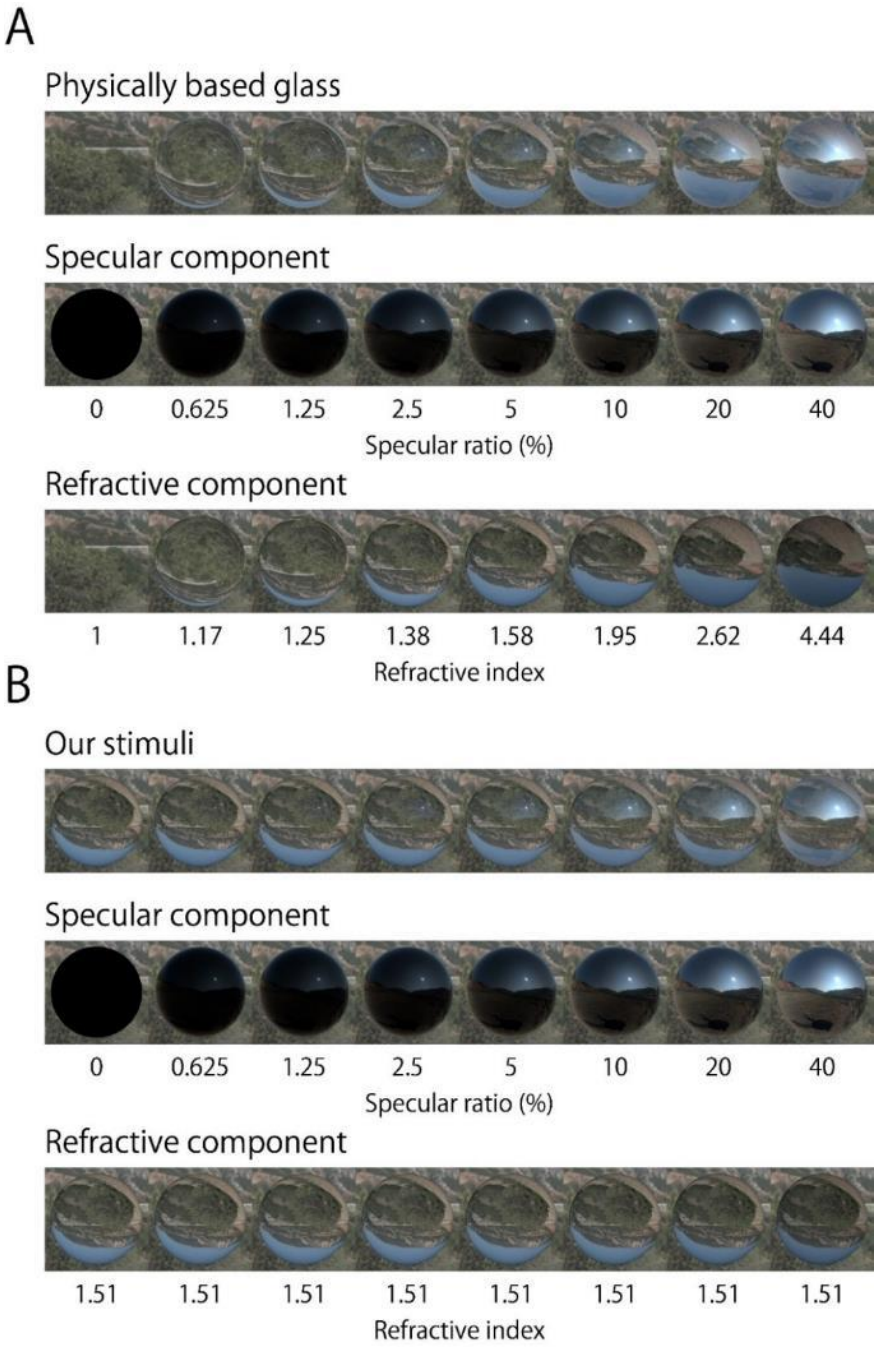


Figure 5.1: Physically based rendering and my stimuli renderings. (A) Physically based rendering changes object refractive distortion along specular intensity. Middle and bottom rows show the specular and refractive components of the image on the top row. Refractive images were rendered by variable refractive index. (B) Top row shows objects which were rendered using method of my experimental stimuli. Middle and bottom rows show the specular and refractive components of the image in the top row. Refractive images were rendered using a fixed refractive index.

## 5.2. Effect of the light probes

The perceived thickness of objects varied depending on the light probe used. In some cases, response probabilities were consistently high (i.e., Cathedral and Closed bar), and in some other cases, the probabilities were relatively low and showed continuous increase (i.e., Morning and Mountain). In Experiment 1, different light probes were used (Grove and St Peters), and similar conclusions were obtained; the pure specular image induced overestimation and the pure refractive image induced relative underestimation. It is also known that the structure of the surrounding environment affects the appearance of the refractive object (Nefs et al., 2006; Khang et al., 2007; Fleming et al., 2009; Chowdhury et al., 2017). The divergence could be due to the difference in image-based features such as variance of the local RMS contrast and other properties (Zhang et al., 2019). Although I did not find any explanation for the differential effect of light probes. The quantitative information of the light probe used in this experiment is calculated and shown below.

### 5.2.1. The statistical feature of light probe

I have explained the experimental result using variance of RMS contrast in object appearance. Since light probes influence an object's appearance, analysis of light probes may also be useful in explaining thickness perception. One possible method of the analysis of light probe is to decompose the spherical function of the light probe by the sum of its spherical harmonics (Doerschner et al., 2007; Mury et al., 2007).

Spherical harmonics analysis is analogous to a Fourier analysis of planar patterns. The reason why spherical harmonic analysis was applied to the analysis of the light probe is that the light probe is originally spherical (Figure 5.2) and when it is transformed into a plane as shown in Figure 5.3, the frequency response of the light probe changes.

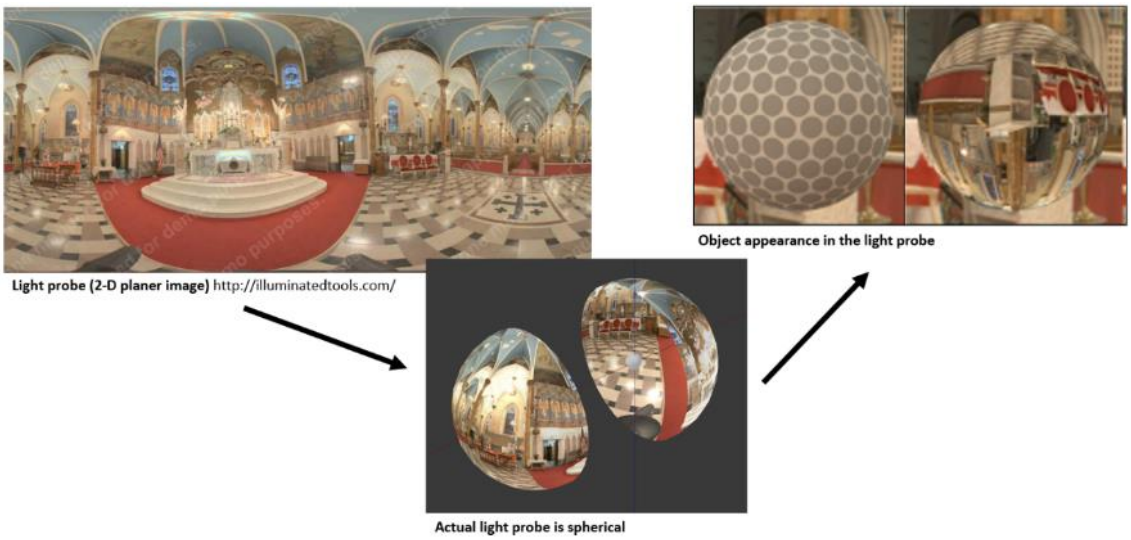


Figure 5.2: The light probe has luminance information. When applied to a computer graphic space by attaching it to a sphere, it creates a natural lighting environment, like 'the direction where the light source is bright'.


Figure 5.3: Planar light probes lose accurate spatial structure. When a light probe of a spherical surface is transformed into a two-dimensional image for Fourier transformation, the left and right edge that should be connected become disconnected. Also, the frequency response changes as the image is stretched closer to the top and bottom edges.

### 5.2.2. Spherical harmonics function and spatial frequency of light probes

The spatial feature harmonics decomposition expresses the luminance at a fix point as a spherical function (Doerschner et al., 2007; Mury et al., 2009; Adams et al., 2018). The spherical function of a fixed point in light-probe space $f(\theta, \varphi)$ can be represented as the sum of its harmonics:

$$f(\theta, \varphi) = \sum_{l=0}^{\infty} \sum_{m=-l}^{l} f_{l,m} Y_{l,m}(\theta, \varphi)$$

where $\theta$ is the polar angle, and $\varphi$ is the azimuth angle of the planar light probe image (Figure 5.4).

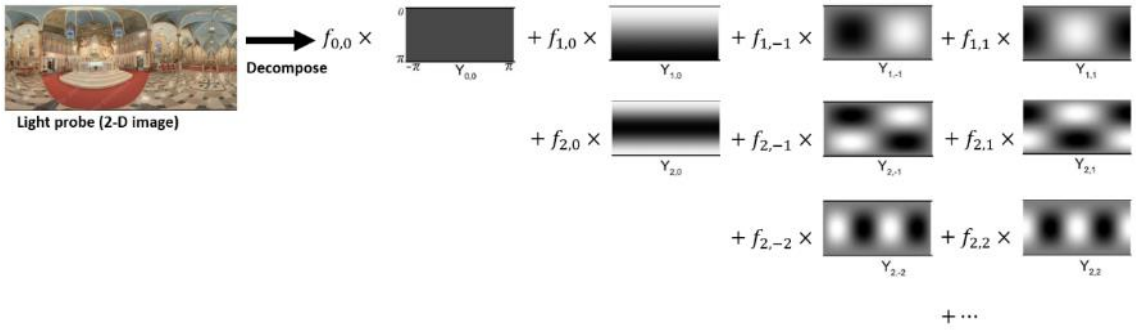


Figure 5.4: Light probe decomposition using a spherical harmonics function. The spatial structure of the luminance light probe can be decomposed with a basis function $Y_{l,m}$ and its coefficient $f_{l,m}$.

The real-value basis functions are defined as

$$Y_{l,m}(\theta, \varphi) = \begin{cases} \sqrt{2} K_{l,m} \cos(m\varphi) P_{l,m}(\cos\theta), & m > 0, \\ \sqrt{2} K_{l,-m} \sin(-m\varphi) P_{l,-m}(\cos\theta), & m < 0, \\ K_{l,0} P_{l,0} \cos(\theta), & m = 0, \end{cases}$$

where $P_{l,m}$ are the associated Legendre polynomials and $K_{l,m}$ are normalization factors. The coefficients $f_{l,m}$ indicate which intensity of the basis function $Y_{l,m}(\theta, \varphi)$ can be calculated as

$$f_{l,m} = \int_{\varphi=0}^{2\pi} \int_{\theta=0}^{\pi} f(\theta, \varphi) Y_{l,m}(\theta, \varphi) \sin(\theta) \, d\theta d\varphi$$

where the order $l$ is $l \geq 0$ and $-l \leq m \leq l$. The order $l$ shows the frequency and $m$ shows the phase of the basis function. Then the power of specific frequency $d_l$ can be calculated as

$$d_l = \sqrt{\sum_{m=-l}^{l} f_{l,m}^2}$$

Figure 5.5 shows the spatial frequency distribution of light probes which were used in above experiments (chapter 2 and 3).

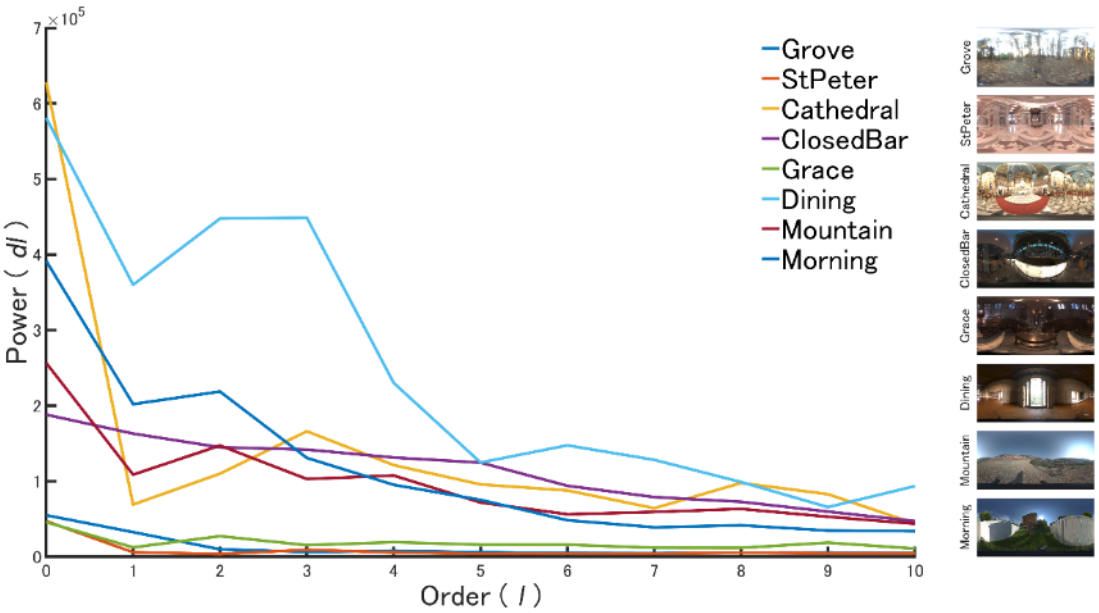


Figure 5.5: Spherical harmonic power ($d_l$) of the light probe components up to tenth order $l$. Eight light probes were used in above experiment (chapter 2 and 3).

### 5.2.3. Metrics using the spherical harmonics analysis

It is known that light probes affect the perceived gloss of opaque objects (Fleming et al., 2003; Mury et al., 2007; Faul, 2019, 2021; Zhang et al., 2019). And Zhang et al. (2019) distinguished the two quantitative values directly related to gloss perception. These values are named Diffuseness and Brilliance. Both are determined from coefficients of the spherical harmonics of light probe. Both are calculated as

$$\text{Diffuseness} = 1 - \frac{d_{l=1}}{d_{l=0}} / \sqrt{3} \ ,$$

$$\text{Brilliance} = \frac{\sum_{l=3}^{\infty} d_l}{\sum_{l=0}^{\infty} d_l},$$

and the values lie between 0 and 1. Figure 5.6 shows these values for the eight light probes used in this thesis. Also shown are light probes used in previous research as a reference. The values of light probes used in this thesis are similar to the values which were used in previous research. However, these values do not allow some conclusions which can be drawn. In other words, the quantitative characteristics of the light probe for objects containing transparent images cannot be expressed by Diffuseness or Brilliance.

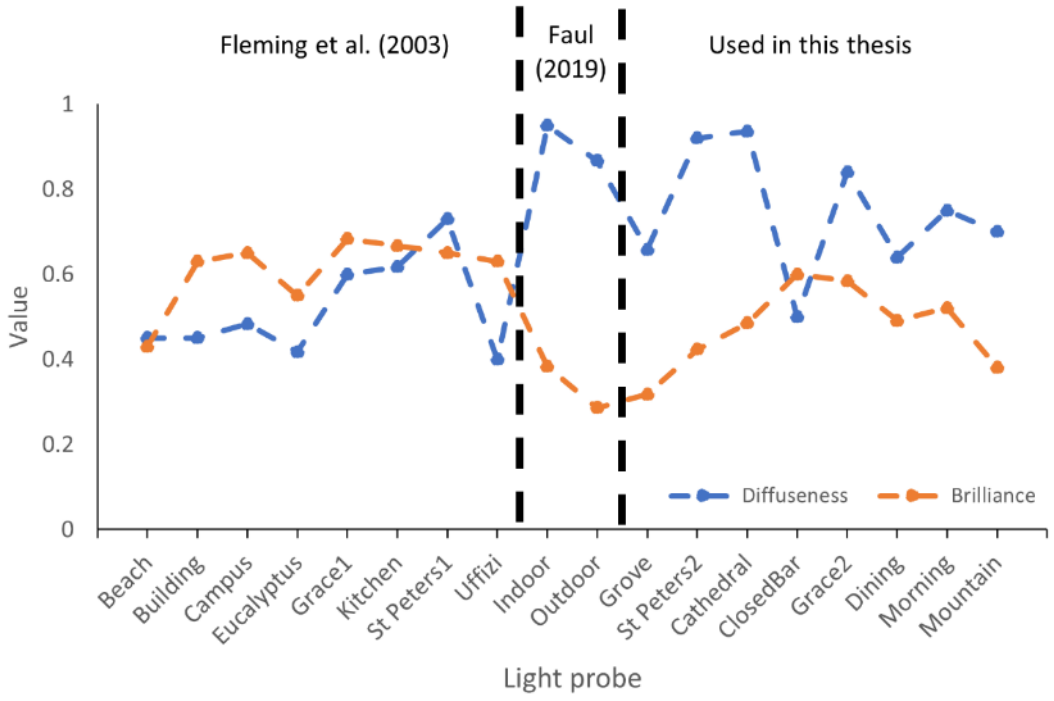


Figure 5.6: Diffuseness and Brilliance of light probes. From the left, the values of ten light probes that were used in Fleming et al. (2003) and in Faul (2019) are shown as a reference. The values of eight light probes used in this thesis (Chapter 2 and 3) are shown on the righthand side. Some names of the light probes are similar (i.e., Grace1 and Grace2), but all of source HDR images are different.

## 5.3. Depth perception through the knowledge of ordinary transparent objects

The experiments in chapter 2 showed that transparent properties decrease thickness perception, while specular reflections increase thickness perception. In addition, the

experiments in chapter 3 showed that adding 5-10% gloss to a transparent object caused it to be perceived as having the same thickness as a matte object.

The reason for the above perception may be that transparent objects with 5-10% specular reflection are commonly seen in daily life (e.g., common glass, transparent resin, diamonds), and a priori knowledge may have occurred so that they are perceived as the correct thickness. With this a priori knowledge, transparent objects with a 5-10% of specular reflection could be perceived as similar in thickness to matte objects with a stable thickness cue called shading.

## 5.4. The difference between surface appearance of specular reflection and transparent reflection

Specular reflections generate image distortions of the surrounding light field, but in a different way to refractive objects; the images of the surrounding light field are flipped upside down through refractive objects (Kim and Marlow, 2016; Tamura et al., 2018). This means that a simple common model may help shape perception. The specularly reflective image mainly reflects the light probe behind the observer, whereas the transparent image mainly shows the light probe on the far side behind the object. Since most light probes have similar characteristics in the front and back, the reflected images are similar except for the fact that they are inverted. However, there is a difference between the reflection images of specular objects and transparent objects when compared precisely. The reflection of shiny objects depends on the object's 3D shape, surface roughness, and lighting environment (Fleming et al., 2004; Adato et al., 2007; Fleming, 2014; Mooney and Anderson, 2014; Dövencioğlu et al., 2017). In addition to the above factors, the transparent image varies with the refractive index and the distance between the object and the background (Todd and Mingolla, 1983; Fleming et al., 2011b; Schlüter and Faul, 2014; Todd and Norman, 2019). Due to the above differences, it is not sufficient to simply flip the image of a transparent object upside down to estimate the shape of a transparent object, and then apply a model that can explain the shape of diffuse reflective or shiny objects (e.g., using orientation maps). To solve this problem, it would be effective to use an index that can directly analyze the image of an object with transparent properties, such as the variance of local RMS contrast.

## 5.5. Comparison with theoretically expected depth cues

Information about thickness and solidity can be obtained from binocular stereopsis, motion parallax, and tactile sensation. These cues are powerful (Ernst and Banks, 2002; Willigen et al., 2010; Lovell and Harris, 2012; Chen and Allison, 2013; Marlow and Anderson, 2015). In

chapter 2, I tested the effect of motion and compared it with the static image condition. The perceived thickness was more accurate in the motion condition indicating the strength of motion as a cue for perception. However, even in the static condition, there was still a perceptual bias in which glossy areas appeared to be thicker and transparent areas appeared to be thinner. In other words, even in the presence of strong and direct stereoscopic cues, there is still a perceptual bias due to image cues.

Pictorial cues also contribute to the perception of three-dimensional shape. These cues include shading and texture gradients. These pictorial cues are theoretically expected to be depth cues because of their geometric properties (Ramachandran, 1988; Todd and Thaler, 2010; Fleming et al., 2011a). These geometrically plausible cues implicitly assume that the visual system performs an inverse optics calculation (Fleming, 2014; Marlow and Anderson, 2015). In the case of the shading, the gradient occurs when a solid homogeneous surface is illuminated from one side, so the inverse presumption is that the shading is suggestive of the depth. In the case of the texture gradients, when a solid homogeneous textured surface has a depth gradient, the farther area of the object from the observer would became finer in their retinal image. So, conversely, texture gradients can be a cue to depth. Although these logical predictions are very reasonable, it is not clear whether the brain actually employs such a computational strategy.

It is possible that the variance of local RMS contrast is performed by the brain. Because it is much simpler than the inverse optics calculation (Srinath et al., 2021), and the two-step filtering is physiologically feasible. The same is true for the orientation map of Fleming et al. in that it is simpler than the calculation of inverse optics (Fleming et al., 2004, 2009, 2011a). On the other hand, variance of local RMS contrast is not theoretically predictable to be a geometrical three-dimensional cue. Nevertheless, it is considered to be a statistically and empirically useful cue that the brain has learned to rely upon.

### 5.6. Investigating the material perception through the depth perception

As mentioned in the introduction of chapter 1, an object's image is comprised of three factors: shape, material, and lighting. Perceiving these factors would be influenced by each other. In this study, I focused on shape and found that the material and lighting environment altered the shape perception. Regarding the material, it was confirmed that each category such as diffuse reflection, glossy reflection, and transparency had a certain effect on thickness perception. Those effects were explained by simple image statistics – variance of the image's local RMS contrast. As for the lighting environment, however, no clear index has been found

to explain the effect of various materials on thickness perception consistently. It may be possible to find this index by investigating the relationship between lighting environment and material, as Pont et al. have found for the objects other than those with diffuse or glossy reflections (Zhang and Pont, 2018, Zhang et al., 2019).

The paradigm used in this study is particularly important because of its applicability to the other materials and lighting environments. In order to fully understand the influence of shape, material, and illumination, it would be necessary to conduct with materials other than the surface materials discussed in this study (matte, specular, and transparent). For example, fabrics, wooden surfaces, rubber, and structural color (e.g., iridescence, pearl) would be popular materials. It also should be tested with other light probes including dynamic environments. For example, some observers may examine glossiness by moving their hands in front of the metallic objects to see specular reflections. No matter what the materials and lighting environments, the objects have three-dimensional shape. Therefore, the experimental paradigm of perceiving depth would be applicable to those materials and lighting environments.

If the variance of local RMS contrast model can be applied to other surface materials than the one used in this study, it can be used as an index to explain thickness perception independent of the material. There is a possibility that we can intentionally control the visibility of an object based on such an index. For example, it is possible to take a picture of an object with a camera and calculate the variance of local RMS contrast in real time. Based on the variance of local RMS contrast, we can use it as a reference to adjust the operable factors of either the object's shape, surface material, or illuminations. This index allows us to automatically control the perceived thickness of object without depending on expert observers which contributes to the cost effectiveness of manufacturing and designs.

## 6. Conclusion

We explored the visual perception of shape in computer-generated objects with different surface optics. Our results suggest that the shape of purely refractive objects tends to be strongly underestimated, compared with surfaces with specular reflectance. Also, our results indicated that observed overestimation and underestimation achieved an equilibrium at the specular component of 5%, consistent with the natural optical properties of glass and water. This coincidence suggests that the human visual system is tuned to correctly recognize the shapes of solid transparent objects as they have specific specular ratios. Perceived thickness of the objects was well characterized by a simple image cue – variance of local RMS contrast

of the images. Simple image statistics would be beneficial to understand the visual system and the applications for manufacture and design.

## Acknowledgements

I would like to thank my supervisor Kowa Koida for realizing me the interest of scientific research. He also gave me vast knowledge and countless discussion. I greatly treasure this six years' experience in his laboratory. I would like to thank my external supervisor: Juno Kim for his warm supporting, discussion, and giving me great chance to study in University of New South Wales for two months; Michiteru Kitazaki for fruitful comment and giving me great chance to study about virtual reality environment as my internship; Hirohiko Kaneko for fruitful comment. Finally, I would like to also thank Leading program of Toyohashi University of technology and 3s-foundation for much scholarship. They were my lifeline of my study and life.

## Reference

Adams, W. J., Kucukoglu, G., Landy, M. S., and Mantiuk, R. K. (2018). Naturally glossy: Gloss perception, illumination statistics, and tone mapping. *J. Vis.* 18, 4. doi:10.1167/18.13.4.

Adato, Y., Vasilyev, Y., Ben-Shahar, O., and Zickler, T. (2007). Toward a theory of shape from specular flow. *Proc. IEEE Int. Conf. Comput. Vis.* doi:10.1109/ICCV.2007.4408883.

Ascher, S. (2019). *The Filmmaker's Handbook*. 5th editio. Plume.

Belhumeur, P. N., Kriegman, D. J., and Yuille, A. L. (1999). The Bas-Relief Ambiguity. *Int. J. Comput. Vis.* 35, 33–44. doi:10.1023/A:1008154927611.

Bernhard, M., Waldner, M., Plank, P., Solteszova, V., and Viola, I. (2016). The Accuracy of Gauge-Figure Tasks in Monoscopic and Stereo Displays. *IEEE Comput. Graph. Appl.* 36, 56–66. doi:10.1109/MCG.2016.45.

Bex, P. J., and Makous, W. (2002). Spatial frequency, phase, and the contrast of natural images. *J. Opt. Soc. Am. A* 19, 1096–1106. doi:10.1364/JOSAA.19.001096.

Blake, A., and Bulthoff, H. (1991). Shape from specularities: computation and psychophysics. *Philos. Trans. R. Soc. London. Ser. B Biol. Sci.* 331, 237–252. doi:10.1098/rstb.1991.0012.

Blake, A., and Bülthoff, H. (1990). Does the brain know the physics of specular reflection? *Nature* 343, 165–168. doi:10.1038/343165a0.

Brown, B. (2016). *Cinematography: Theory and Practice*. 3rd editio. Routledge.

Chen, J., and Allison, R. S. (2013). Shape Perception of Thin Transparent Objects with Stereoscopic Viewing. *ACM Trans. Appl. Percept.* 10. doi:10.1145/2506206.2506208.

Chowdhury, N. S., Marlow, P. J., and Kim, J. (2017). Translucency and the perception of shape.

*J. Vis.* 17, 1–17. doi:10.1167/17.3.17.

De Haan, E., Erens, R. G. F., and Noest, A. J. (1995). Shape from shaded random surfaces. *Vision Res.* 35, 2985–3001. doi:10.1016/0042-6989(95)00050-A.

DMMLabo株式会社 (2016). 2016年3月：スマートフォン端末利用動向調査. *DMM研究所*. Available at: https://mmdlabo.jp/press_release/detail_1536.html.

Doerschner, K., Boyaci, H., and Maloney, L. T. (2007). Testing limits on matte surface color perception in three-dimensional scenes with complex light fields. *Vision Res.* 47, 3409–3423. doi:https://doi.org/10.1016/j.visres.2007.09.020.

Dövencioğlu, D. N., Ben-shahar, O., Barla, P., Doerschner, K., and Department (2017). Specular motion and 3D shape estimation. *J. Vis.* 17(6), 1–15. doi:10.1167/17.6.3.doi.

Dövencioğlu, D. N., van Doorn, A., Koenderink, J., and Doerschner, K. (2018). Seeing through transparent layers. *J. Vis.* 18, 1–25. doi:10.1167/18.9.25.

Dövencioğlu, D. N., Wijntjes, M. W. A., Ben-Shahar, O., and Doerschner, K. (2015). Effects of surface reflectance on local second order shape estimation in dynamic scenes. *Vision Res.* 115, 218–230. doi:https://doi.org/10.1016/j.visres.2015.01.008.

Ernst, M. O., and Banks, M. S. (2002). Humans integrate visual and haptic information in a statistically optimal fashion. *Nature* 415, 429–433. doi:10.1038/415429a.

Faul, F. (2019). The influence of Fresnel effects on gloss perception. *J. Vis.* 19, 1. doi:10.1167/19.13.1.

Faul, F. (2021). Perceived roughness of glossy objects: The influence of Fresnel effects and correlated image statistics. *J. Vis.* 21, 1–29. doi:10.1167/jov.21.8.1.

Fleming, R. W. (2014). Visual perception of materials and their properties. *Vision Res.* 94, 62–75. doi:10.1016/j.visres.2013.11.004.

Fleming, R. W., Dror, R. O., and Adelson, E. H. (2003). Real-world illumination and the perception of surface reflectance properties. *J. Vis.* 3, 347–368. doi:10:1167/3.5.3.

Fleming, R. W., Holtmann-Rice, D., and Bülthoff, H. H. (2011a). Estimation of 3D shape from image orientations. *Proc. Natl. Acad. Sci. U. S. A.* 108, 20438–20443. doi:10.1073/pnas.1114619109.

Fleming, R. W., Jäkel, F., and Maloney, L. T. (2011b). Visual perception of thick transparent materials. *Psychol. Sci.* 22, 812–820. doi:10.1177/0956797611408734.

Fleming, R. W., Torralba, A., and Adelson, E. H. (2004). Specular reflections and the perception of shape. *J. Vis.* 4, 798–820. doi:10.1167/4.9.10.

Fleming, R. W., Torralba, A., and Adelson, E. H. (2009). Shape from Sheen. Available at: https://dspace.mit.edu/handle/1721.1/49511 [Accessed January 23, 2020].

Freeman, J., Ziemba, C. M., Heeger, D. J., Simoncelli, E. P., and Movshon, J. A. (2013). A functional and perceptual signature of the second visual area in primates. *Nat. Neurosci.*

16, 974–981. doi:10.1038/nn.3402.

Hashimoto, K. (2020). 色と顔料の世界. sankyou-syuppann.

Hecht, E. (2002). *Optics*. Pearson Education India.

Ho, Y.-X., Landy, M. S., and Maloney, L. T. (2008). Conjoint Measurement of Gloss and Surface Texture. *Psychol. Sci.* 19, 196–204. doi:10.1111/j.1467-9280.2008.02067.x.

Hubel, D. H., and Wiesel, T. N. (1962). Receptive fields, binocular interaction and functional architecture in the cat's visual cortex. *J. Physiol.* 160, 106–154. doi:https://doi.org/10.1113/jphysiol.1962.sp006837.

Kao Corporation (2020). New Makeup Technology Inconspicuously Smoothens Nasolabial Folds by Simple Application. Available at: https://www.kao.com/global/en/news/rd/2020/20201210-001/ [Accessed December 1, 2021].

Kawabe, T., and Kogovšek, R. (2017). Image deformation as a cue to material category judgment. *Sci. Rep.* 7. doi:10.1038/srep44274.

Kawabe, T., Maruya, K., Fleming, R. W., and Nishida, S. (2015). Seeing liquids from visual motion. *Vision Res.* 109, 125–138. doi:https://doi.org/10.1016/j.visres.2014.07.003.

Kawashima, M., and Hikima, R. (2015). Effects of cosmetics on emotional states in women. *Japanese Psychol. Assoc.* 79, 3EV-096-3EV – 096. doi:10.4992/pacjpa.79.0_3EV-096.

Khang, B. G., Koenderink, J. J., and Kappers, A. M. L. (2007). Shape from shading from images rendered with various surface types and light fields. *Perception* 36, 1191–1213. doi:10.1068/p5807.

Kim, J., and Anderson, B. L. (2010). Image statistics and the perception of surface gloss and lightness. *J. Vis.* 10, 1–17. doi:10.1167/10.9.3.

Kim, J., Khuu, S., and Palmisano, S. (2016a). Vection depends on perceived surface properties. *Attention, Perception, Psychophys.* 78, 1163–1173. doi:10.3758/s13414-016-1076-9.

Kim, J., and Marlow, P. J. (2016). Turning the World Upside Down to Understand Perceived Transparency. *Iperception.* 7, 204166951667156. doi:10.1177/2041669516671566.

Kim, J., Tan, K., and Chowdhury, N. S. (2016b). Image statistics and the fine lines of material perception. *Iperception.* 7, 1–11. doi:10.1177/2041669516658047.

Koenderink, J. J., and van Doorn, A. J. (1992). Surface shape and curvature scales. *Image Vis. Comput.* 10, 557–564. doi:10.1016/0262-8856(92)90076-F.

Kunsberg, B., and Zucker, S. W. (2014). How shading constrains surface patches without knowledge of light sources. *SIAM J. Imaging Sci.* 7, 641–668. doi:10.1137/13092647X.

LEE, M., SHIMADA, R., and NARITA, Y. (2018). The Effect of Combination of Different Materials on "OSHARE" Feeling of Objects. *Trans. Japan Soc. Kansei Eng.* 17, 177–186.

Lovell, P. G., and Harris, J. M. (2012). Optimal integration of shading and binocular disparity

for depth perception. 12, 1–18. doi:10.1167/12.1.1.Introduction.

Marlow, P. J., and Anderson, B. L. (2015). Material properties derived from three-dimensional shape representations. *Vision Res.* 115, 199–208. doi:10.1016/j.visres.2015.05.003.

Marlow, P. J., Kim, J., and Anderson, B. L. (2012). The Perception and Misperception of Specular Surface Reflectance. *Curr. Biol.* 22, 1909–1913. doi:https://doi.org/10.1016/j.cub.2012.08.009.

Marr, D. (1982). *Vision: A Computational Investigation into the Human Representation and Processing of Visual Information*. The MIT Press doi:10.7551/mitpress/9780262514620.001.0001.

Mooney, S. W. J., and Anderson, B. L. (2014). Specular image structure modulates the perception of three-dimensional shape. *Curr. Biol.* 24, 2737–2742. doi:10.1016/j.cub.2014.09.074.

Motoyoshi, I., Nishida, S., Sharan, L., and Adelson, E. H. (2007). Image statistics and the perception of surface qualities. *Nature* 447, 206–209. doi:10.1038/nature05724.

Mury, A. A., Pont, S. C., and Koenderink, J. J. (2007). Light field constancy within natural scenes. *Appl. Opt.* 46, 7308–7316. doi:10.1364/AO.46.007308.

Mury, A. A., Pont, S. C., and Koenderink, J. J. (2009). Structure of light fields in natural scenes. *Appl. Opt.* 48, 5386–5395. doi:10.1364/AO.48.005386.

Nefs, H. T., Koenderink, J. J., and Kappers, A. M. L. (2006). Shape-from-shading for matte and glossy objects. *Acta Psychol. (Amst).* 121, 297–316. doi:10.1016/j.actpsy.2005.08.001.

Nishida, S., and Shinya, M. (1998). Use of image-based information in judgments of surface-reflectance properties. *J. Opt. Soc. Am. A* 15, 2951–2964. doi:10.1364/josaa.15.002951.

Norman, J. F., Todd, J. T., and Phillips, F. (1995). The perception of surface orientation from multiple sources of optical information. *Percept. Psychophys.* 57, 629–636. doi:10.3758/BF03213268.

Ohara, M., Kim, J., and Koida, K. (2020). The Effect of Material Properties on the Perceived Shape of Three-Dimensional Objects. *Iperception.* 11, 1–14. doi:10.1177/2041669520982317.

Olkkonen, M., and Brainard, D. H. (2011). Joint effects of illumination geometry and object shape in the perception of surface reflectance. *Iperception.* 2, 1014–1034. doi:10.1068/i0480.

Pelli, D. G., and Bex, P. (2013). Measuring contrast sensitivity. *Vision Res.* 90, 10–14. doi:https://doi.org/10.1016/j.visres.2013.04.015.

Polyanskiy, M. (2008). RefractiveIndex.INFO. Available at: https://refractiveindex.info/.

Ramachandran, V. S. (1988). Perception of the shape from shading. *Nature* 331, 163–166.

Richards, W. (1988). *Natural computation*. MIT Press.

Rieger, J. W., Gegenfurtner, K. R., Schalk, F., Koechy, N., Heinze, H.-J., and Grueschow, M. (2013). BOLD responses in human V1 to local structure in natural scenes: Implications for theories of visual coding. *J. Vis.* 13, 19. doi:10.1167/13.2.19.

Sakai, K., and Finkel, L. H. (1995). Characterization of the Spatial Frequency Spectrum in Perception of Shape-from-Texture.

Savarese, S., Chen, M., and Perona, P. (2004a). *Recovering Local Shape of a Mirror Surface from Reflection of a Regular Grid*. doi:10.1007/978-3-540-24672-5_37.

Savarese, S., Chen, M., and Perona, P. (2005). Local Shape from Mirror Reflections. *Int. J. Comput. Vis.* 64, 31–67. doi:10.1007/s11263-005-1086-x.

Savarese, S., Fei-Fei, L., and Perona, P. (2004b). What Do Reflections Tell Us about the Shape of a Mirror? in *Proceedings of the 1st Symposium on Applied Perception in Graphics and Visualization* APGV '04. (New York, NY, USA: Association for Computing Machinery), 115–118. doi:10.1145/1012551.1012571.

Schlüter, N., and Faul, F. (2014). Are optical distortions used as a cue for material properties of thick transparent objects? *J. Vis.* 14, 1–14. doi:10.1167/14.14.2.doi.

Schlüter, N., and Faul, F. (2019). Visual shape perception in the case of transparent objects. *J. Vis.* 19, 1–36. doi:10.1167/19.4.24.

Shimokawa, T., Nishio, A., Sato, M., Kawato, M., and Komatsu, H. (2019). Computational Model for Human 3D Shape Perception From a Single Specular Image. *Front. Comput. Neurosci.* 13, 10. doi:10.3389/fncom.2019.00010.

Srinath, R., Emonds, A., Wang, Q., Lempel, A. A., Dunn-Weiss, E., Connor, C. E., et al. (2021). Early Emergence of Solid Shape Coding in Natural and Deep Network Vision. *Curr. Biol.* 31, 51-65.e5. doi:https://doi.org/10.1016/j.cub.2020.09.076.

Tamura, H., Higashi, H., and Nakauchi, S. (2018). Dynamic Visual Cues for Differentiating Mirror and Glass. *Sci. Rep.* 8, 1–12. doi:10.1038/s41598-018-26720-x.

Tobitani, K., Shiraiwa, A., Katahira, K., Nagata, N., Nikata, K., and Arakawa, K. (2021). Modeling of "High-Class Feeling" on a Cosmetic Package Design. *J. Japan Soc. Precis. Eng.* 87, 134–139. doi:10.2493/jjspe.87.134.

Todd, J. T., Egan, E. J. L., and Kallie, C. S. (2015). The darker-is-deeper heuristic for the perception of 3D shape from shading: Is it perceptually or ecologically valid? *J. Vis.* 15, 1–10. doi:10.1167/15.15.2.

Todd, J. T., and Mingolla, E. (1983). Perception of surface curvature and direction of illumination from patterns of shading. *J. Exp. Psychol. Hum. Percept. Perform.* 9, 583–595. doi:10.1037/0096-1523.9.4.583.

Todd, J. T., and Norman, J. F. (2019). Reflections on glass. *J. Vis.* 19, 1–21. doi:10.1167/19.4.26.

Todd, J. T., Oomes, A. H. J., Koenderink, J. J., and Kappers, A. M. L. (2004). The Perception of

Doubly Curved Surfaces from Anisotropic Textures. *Psychol. Sci.* 15, 40–46. doi:10.1111/j.0963-7214.2004.01501007.x.

Todd, J. T., and Thaler, L. (2010). The perception of 3D shape from texture based on directional width gradients. *J. Vis.* 10. doi:10.1167/10.5.17.

Vangorp, P., Laurijssen, J., and Dutré, P. (2007). The influence of shape on the perception of material reflectance. *Proc. ACM SIGGRAPH Conf. Comput. Graph.* 26, 1–9. doi:10.1145/1275808.1276473.

Wendt, G., Faul, F., Ekroll, V., and Mausfeld, R. (2010). Disparity, motion, and color information improve gloss constancy performance. *J. Vis.* 10, 7. doi:10.1167/10.9.7.

Wijntjes, M. W. A., and Pont, S. C. (2010). Illusory gloss on Lambertian surfaces. *J. Vis.* 10, 1–12. doi:10.1167/10.9.13.

Wilder, J. D., Adams, W. J., and Murray, R. F. (2019). Shape from shading under inconsistent illumination. 19, 1–15. doi:10.1167/19.6.2.

Willigen, R. F. Van Der, Harmening, W. M., Vossen, S., Wagner, H., and van der Willigen, R. F. (2010). Disparity Sensitivity in Man and Owl: Psychophysical Evidence for Equivalent Perception of Shape-From-Stereo. *J. Vis.* 10, 1–11. doi:10.1167/10.1.10.

Zhang, F., de Ridder, H., Barla, P., and Pont, S. (2019). A systematic approach to testing and predicting light-material interactions. *J. Vis.* 19, 1–22. doi:10.1167/19.4.11.

Zhang, F., and Pont, S. C. (2018). Asymmetric perceptual confounds between canonical lightings and materials. 18, 1–19. doi:10.1167/18.11.11.

湯澤幸代, and 吉田耕 (2014). 最近のモーターショーに見る自動車ボディ加飾トレンドと素材変革の調査報告, 塗料の研究. 塗料の研究 156, 32–37.

## Supplemental materials

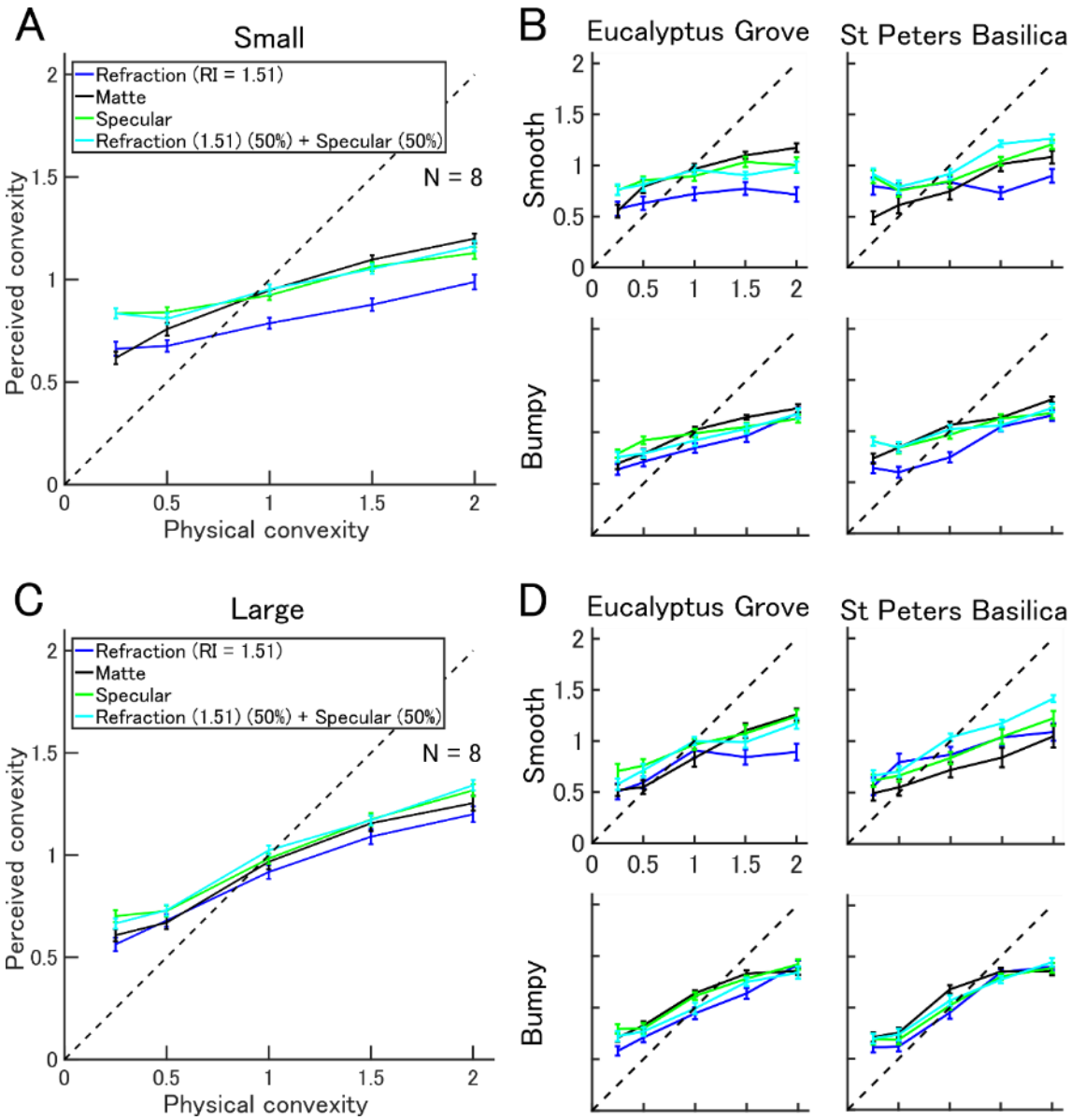


Figure S1: Effect of material properties on perceived convexity for different size stimuli. Format is same as in Figure 2.2. (A, B) Results for the small object of ×0.5 size. (C, D) Results for the large object ×2.0 size.

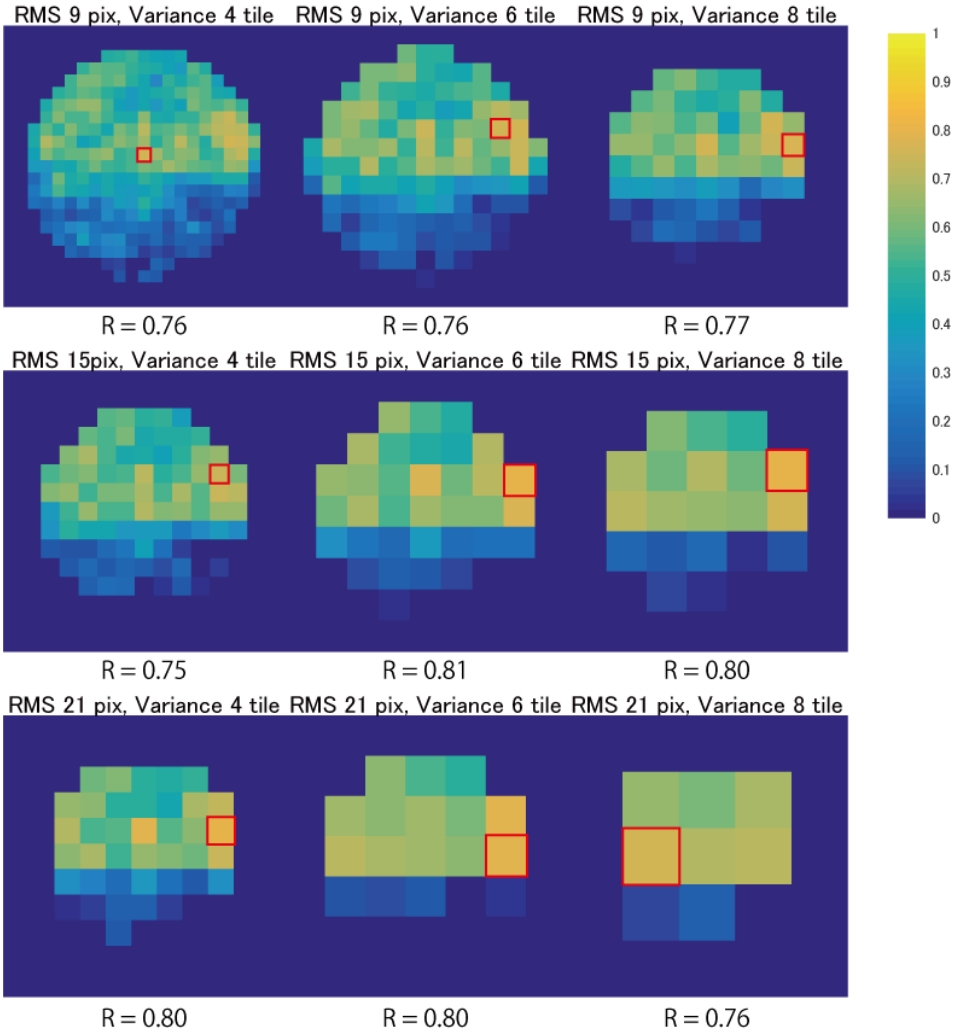


Figure S2: Correlation between 'local' RMS contrast variability and perceived convexity in various RMS pixel and variance tile size. These heat maps were computed in the same way as Figure 4.1E in main text except for the region size. Local RMS contrast was calculated in three different size (9 × 9, 15 × 15, 21 × 21 pixels; 0.61 × 0.61, 1.0 × 1.0, 1.4 × 1.4 deg, respectively), and variance of RMS contrast were calculated in three different regions (4 × 4, 6 × 6, 8 × 8). Red tiles show the area of highest correlation coefficient within each image. The R value on bottom shows the correlation coefficient in red square. As shown in main text, higher correlation was obtained for upper half of the image for all analysis.

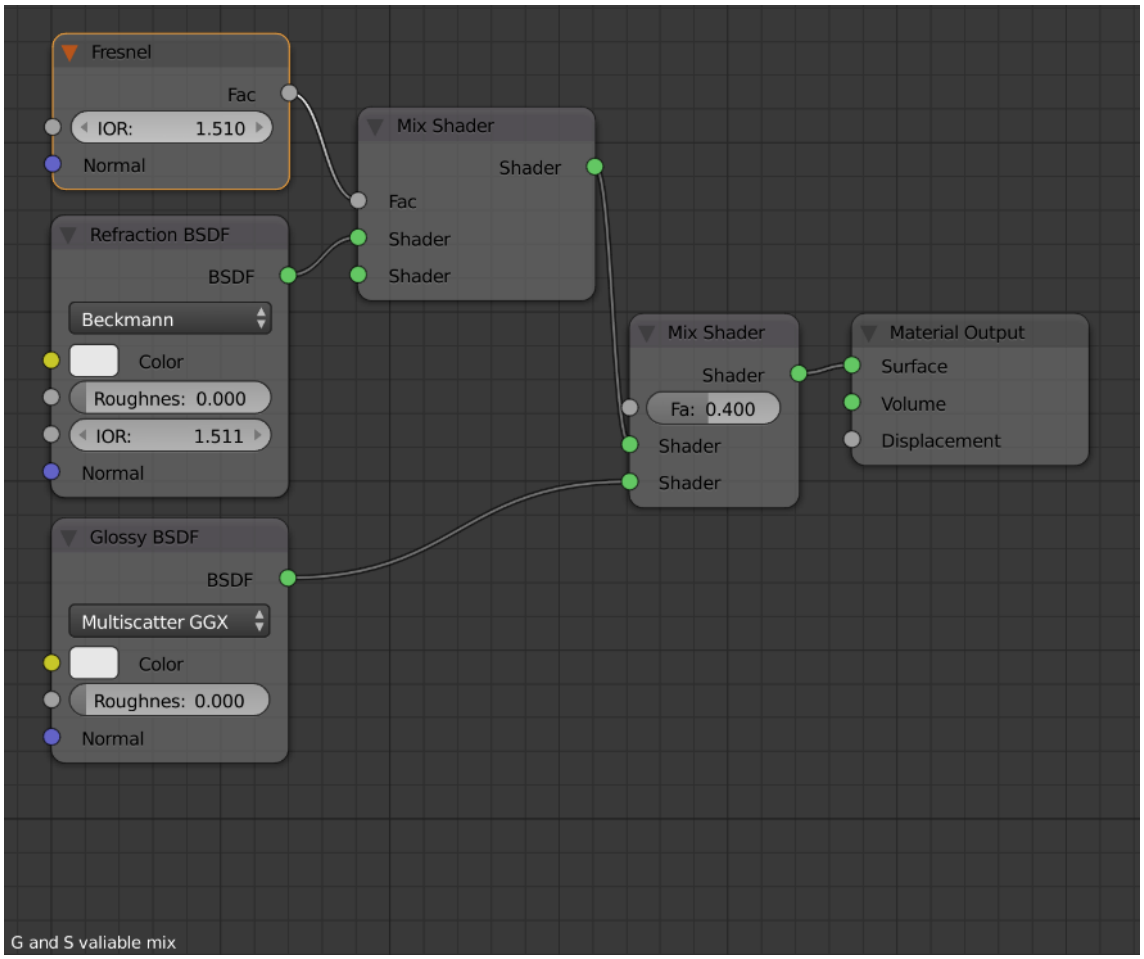


Figure S3: Blender node setup in the Test surface.

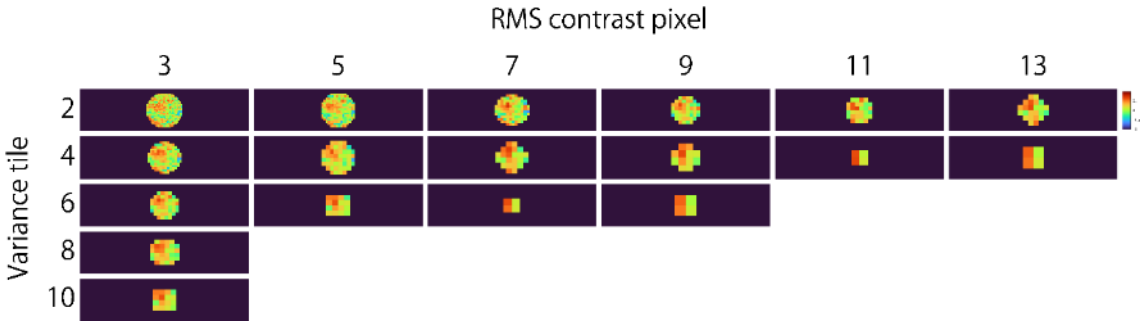


Figure S4: Correlation between various calculation range of local RMS contrast variability and observer response. Heatmap shows the correlation between local RMS contrast variability and experimental result of all six light probes. Horizontal number shows calculation range of local RMS contrast. Vertical number shows calculation range of variance.

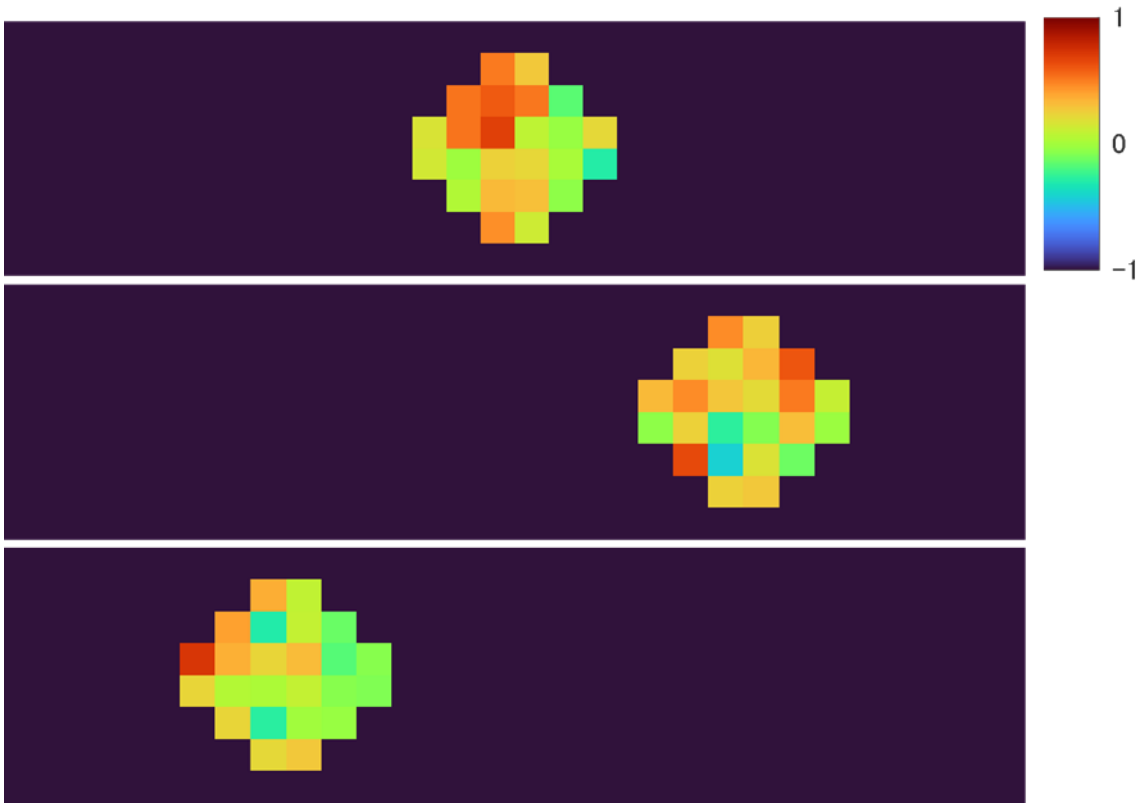


Figure S5: Correlation between various calculation range of local RMS contrast variability and observer response in each object position. Heatmap shows the correlation between local RMS contrast variability and experimental result of average of all six light probes. The position of the object shows center, right end and left end of the oscillating motion.

Table S1: Statistics of experimental results (Figure 2.2)

This table show the result of 4-way (light probe, bump level, physical convexity and material property) anova.

| Source | Sum of squares | d.f. | Mean squares | F | p | Partial $\eta^2$ |
|---|---|---|---|---|---|---|
| Light probe | 0.158 | 1 | 0.158 | 2.04 | 0.153 | 0.001 |
| Bumpiness | 0.037 | 1 | 0.037 | 0.48 | 0.489 | 0.000 |
| Material | 3.933 | 3 | 1.311 | 16.91 | <0.001 | 0.026 |
| Convexity | 112.028 | 1 | 112.028 | 1445.23 | <0.001 | 0.434 |
| Light probe*Bumpiness | 0.119 | 1 | 0.119 | 1.53 | 0.216 | 0.001 |
| Light probe*Material | 0.383 | 3 | 0.128 | 1.65 | 0.177 | 0.003 |
| Light probe*Convexity | 0.837 | 1 | 0.837 | 10.8 | <0.001 | 0.006 |
| Bumpiness*Material | 2.333 | 3 | 0.778 | 10.03 | <0.001 | 0.016 |
| Bumpiness*Convexity | 2.924 | 1 | 2.924 | 37.73 | <0.001 | 0.020 |
| Material*Convexity | 0.633 | 3 | 0.211 | 2.72 | 0.043 | 0.004 |
| Light probe*Bumpiness*Material | 1.027 | 3 | 0.342 | 4.42 | 0.004 | 0.007 |
| Light probe*Bumpiness*Convexity | 0.018 | 1 | 0.018 | 0.24 | 0.627 | 0.000 |
| Light probe*Material*Convexity | 0.160 | 3 | 0.053 | 0.69 | 0.560 | 0.001 |
| Bumpiness*Material*Convexity | 2.380 | 3 | 0.793 | 10.23 | <0.001 | 0.016 |
| Light probe*Bumpiness*Material*Convexity | 0.478 | 3 | 0.159 | 2.06 | 0.104 | 0.003 |
| Error | 146.349 | 1888 | 0.078 | | | |
| Total | 289.030 | 1919 | | | | |

Post-hoc test: Tukey HSD (Refraction (RI = 1.51) vs other 3 surface materials)

| Fig2.2A |
|---|
| p (vs matte) = <0.001 |
| p (vs specular) = <0.001 |
| p (vs refraction (50%) + specular (50%)) = <0.001 |
| |
| Fig2.2B |
| **Eucalyptus Grove - smooth** |
| p (vs matte) = <0.001 |
| p (vs specular) = <0.001 |
| p (vs refraction (50%) + specular (50%)) = <0.001 |
| **Eucalyptus Grove - Bumpy** |
| p (vs matte) = 0.017 |
| p (vs specular) = <0.001 |
| p (vs refraction (50%) + specular (50%)) = 0.896 |
| **St Peters Basilica - smooth** |
| p (vs matte) = 0.949 |
| p (vs specular) = 0.193 |
| p (vs refraction (50%) + specular (50%)) = <0.001 |
| **St Peters Basilica - Bumpy** |
| p (vs matte) = 0.023 |
| p (vs specular) = 0.149 |
| p (vs refraction (50%) + specular (50%)) = 0.109 |

Table S2: Statistics of experimental results (Figure S1)

This table show the result of 5-way (Object size (Large, small), light probe, bump level, physical convexity and material property) anova.

| Source | Sum of squares | d.f. | Mean squares | F | p | Partial $\eta^2$ |
|---|---|---|---|---|---|---|
| Size | 4.364 | 1 | 4.364 | 59.340 | <0.001 | 0.015 |
| Light probe | 0.045 | 1 | 0.045 | 0.620 | 0.433 | 0.000 |
| Bumpiness | 0.391 | 1 | 0.391 | 5.310 | 0.021 | 0.001 |
| Material | 3.717 | 3 | 1.239 | 16.850 | <0.001 | 0.013 |
| Convexity | 147.132 | 1 | 147.132 | 2000.470 | <0.001 | 0.346 |
| Size*Light probe | 0.116 | 1 | 0.116 | 1.580 | 0.209 | 0.000 |
| Size*Bumpiness | 0.157 | 1 | 0.157 | 2.140 | 0.144 | 0.001 |
| Size*Material | 0.698 | 3 | 0.233 | 3.160 | 0.024 | 0.003 |
| Size*Convexity | 9.818 | 1 | 9.818 | 133.480 | <0.001 | 0.034 |
| Light probe*Bumpiness | 0.004 | 1 | 0.004 | 0.050 | 0.816 | 0.000 |
| Light probe*Material | 0.400 | 3 | 0.133 | 1.810 | 0.143 | 0.001 |
| Light probe*Convexity | 0.361 | 1 | 0.361 | 4.910 | 0.027 | 0.001 |
| Bumpiness*Material | 3.795 | 3 | 1.265 | 17.200 | <0.001 | 0.013 |
| Bumpiness*Convexity | 2.629 | 1 | 2.629 | 35.740 | <0.001 | 0.009 |
| Material*Convexity | 1.762 | 3 | 0.587 | 7.980 | <0.001 | 0.006 |
| Size*Light probe*Bumpiness | 0.087 | 1 | 0.087 | 1.190 | 0.276 | 0.000 |
| Size*Light probe*Material | 0.270 | 3 | 0.090 | 1.220 | 0.300 | 0.001 |
| Size*Light probe*Convexity | 0.012 | 1 | 0.012 | 0.160 | 0.692 | 0.000 |
| Size*Bumpiness*Material | 0.089 | 3 | 0.030 | 0.400 | 0.750 | 0.000 |
| Size*Bumpiness*Convexity | 0.104 | 1 | 0.104 | 1.410 | 0.235 | 0.000 |
| Size*Material*Convexity | 1.136 | 3 | 0.379 | 5.150 | 0.002 | 0.004 |
| Light probe*Bumpiness*Material | 0.556 | 3 | 0.185 | 2.520 | 0.056 | 0.002 |
| Light probe*Bumpiness*Convexity | 0.003 | 1 | 0.003 | 0.050 | 0.830 | 0.000 |
| Light probe*Material*Convexity | 0.510 | 3 | 0.170 | 2.310 | 0.074 | 0.002 |
| Bumpiness*Material*Convexity | 3.761 | 3 | 1.254 | 17.050 | <0.001 | 0.013 |
| Size*Light probe*Bumpiness*Material | 0.360 | 3 | 0.120 | 1.630 | 0.180 | 0.001 |
| Size*Light probe*Bumpiness*Convexity | 0.138 | 1 | 0.138 | 1.880 | 0.171 | 0.000 |
| Size*Light probe*Material*Convexity | 0.262 | 3 | 0.087 | 1.190 | 0.313 | 0.001 |
| Size*Bumpiness*Material*Convexity | 0.133 | 3 | 0.044 | 0.600 | 0.612 | 0.000 |
| Light probe*Bumpiness*Material*Convexity | 0.526 | 3 | 0.175 | 2.380 | 0.068 | 0.002 |
| Size*Light probe*Bumpiness*Material*Convexity | 0.266 | 3 | 0.089 | 1.210 | 0.306 | 0.001 |
| Error | 277.721 | 3776 | 0.074 | | | |
| Total | 485.801 | 3839 | | | | |

Post-hoc test: Tukey HSD (Refraction (RI = 1.51) vs other 3 surface materials)

| FigS1A |
|---|
| p (vs matte) = <0.001 |
| p (vs specular) = <0.001 |
| p (vs refraction (50%) + specular (50%)) = <0.001 |
| |
| FigS1B |
| **Eucalyptus Grove - smooth** |
| p (vs matte) = <0.001 |
| p (vs specular) = <0.001 |
| p (vs refraction (50%) + specular (50%)) = <0.001 |
| **Eucalyptus Grove - Bumpy** |
| p (vs matte) = 0.359 |
| p (vs specular) = 0.368 |
| p (vs refraction (50%) + specular (50%)) = 0.992 |
| **St Peters Basilica - smooth** |
| p (vs matte) = 1 |
| p (vs specular) = 0.018 |
| p (vs refraction (50%) + specular (50%)) = <0.001 |
| **St Peters Basilica - Bumpy** |
| p (vs matte) = <0.001 |
| p (vs specular) = <0.001 |
| p (vs refraction (50%) + specular (50%)) = <0.001 |

| FigS1C |
|---|
| p (vs matte) = 0.269 |
| p (vs specular) = <0.001 |
| p (vs refraction (50%) + specular (50%)) = <0.001 |
| |
| FigS1D |
| **Eucalyptus Grove - smooth** |
| p (vs matte) = 0.433 |
| p (vs specular) = <0.001 |
| p (vs refraction (50%) + specular (50%)) = 0.019 |
| **Eucalyptus Grove - Bumpy** |
| p (vs matte) = 0.233 |
| p (vs specular) = 0.118 |
| p (vs refraction (50%) + specular (50%)) = 1 |
| **St Peters Basilica - smooth** |
| p (vs matte) = 0.024 |
| p (vs specular) = 1 |
| p (vs refraction (50%) + specular (50%)) = 0.068 |
| **St Peters Basilica - Bumpy** |
| p (vs matte) = 0.845 |
| p (vs specular) = 1 |
| p (vs refraction (50%) + specular (50%)) = 0.999 |

Post-hoc test: Tukey HSD (flattest (convexity = 0.25) matte object vs flattest specular object)

| | p value |
|---|---|
| FigS1A | <0.001 |
| FigS1B | |
| Eucalyptus Grove - smooth | 1 |
| Eucalyptus Grove - Bumpy | 1 |
| St Peters Basilica - smooth | 0.003 |
| St Peters Basilica - Bumpy | 1 |
| | |
| FigS1C | 0.923 |
| FigS1D | |
| Eucalyptus Grove - smooth | 1 |
| Eucalyptus Grove - Bumpy | 1 |
| St Peters Basilica - smooth | 1 |
| St Peters Basilica - Bumpy | 1 |

Table S3: Statistics of experimental results (Figure 2.3)

This table show the result of 5-way (Object position (Center, Left/Light), light probe, bump level, physical convexity and material property) anova.

| Source | Sum of squares | d.f. | Mean squares | F | p | Partial $\eta^2$ |
|---|---|---|---|---|---|---|
| Position | 0.075 | 1 | 0.075 | 0.870 | 0.350 | <0.001 |
| Light probe | 1.699 | 1 | 1.699 | 19.690 | <0.001 | 0.003 |
| Bumpiness | 2.166 | 1 | 2.166 | 25.100 | <0.001 | 0.004 |
| Material | 17.438 | 3 | 5.813 | 67.370 | <0.001 | 0.034 |
| Convexity | 36.215 | 1 | 36.215 | 419.750 | <0.001 | 0.069 |
| Position*Light probe | 0.012 | 1 | 0.012 | 0.140 | 0.709 | <0.001 |
| Position*Bumpiness | 0.194 | 1 | 0.194 | 2.250 | 0.133 | <0.001 |
| Position*Material | 0.106 | 3 | 0.035 | 0.410 | 0.746 | <0.001 |
| Position*Convexity | 1.805 | 1 | 1.805 | 20.930 | <0.001 | 0.004 |
| Light probe*Bumpiness | 0.146 | 1 | 0.146 | 1.690 | 0.193 | <0.001 |
| Light probe*Material | 3.194 | 3 | 1.065 | 12.340 | <0.001 | 0.006 |
| Light probe*Convexity | 1.443 | 1 | 1.443 | 16.720 | <0.001 | 0.003 |
| Bumpiness*Material | 7.450 | 3 | 2.483 | 28.780 | <0.001 | 0.015 |
| Bumpiness*Convexity | 0.490 | 1 | 0.490 | 5.680 | 0.017 | <0.001 |
| Material*Convexity | 2.968 | 3 | 0.989 | 11.470 | <0.001 | 0.006 |
| Position*Light probe*Bumpiness | 0.005 | 1 | 0.005 | 0.050 | 0.815 | <0.001 |
| Position*Light probe*Material | 0.145 | 3 | 0.048 | 0.560 | 0.640 | <0.001 |
| Position*Light probe*Convexity | 0.208 | 1 | 0.208 | 2.410 | 0.120 | <0.001 |
| Position*Bumpiness*Material | 0.251 | 3 | 0.084 | 0.970 | 0.406 | <0.001 |
| Position*Bumpiness*Convexity | 0.004 | 1 | 0.004 | 0.040 | 0.836 | <0.001 |
| Position*Material*Convexity | 0.219 | 3 | 0.073 | 0.850 | 0.467 | <0.001 |
| Light probe*Bumpiness*Material | 0.515 | 3 | 0.172 | 1.990 | 0.113 | <0.001 |
| Light probe*Bumpiness*Convexity | 0.077 | 1 | 0.078 | 0.900 | 0.343 | <0.001 |
| Light probe*Material*Convexity | 0.519 | 3 | 0.173 | 2.000 | 0.111 | <0.001 |
| Bumpiness*Material*Convexity | 4.002 | 3 | 1.334 | 15.460 | <0.001 | 0.008 |
| Position*Light probe*Bumpiness*Material | 0.033 | 3 | 0.011 | 0.130 | 0.945 | <0.001 |
| Position*Light probe*Bumpiness*Convexity | 0.008 | 1 | 0.008 | 0.100 | 0.755 | <0.001 |
| Position*Light probe*Material*Convexity | 0.181 | 3 | 0.060 | 0.700 | 0.552 | <0.001 |
| Position*Bumpiness*Material*Convexity | 0.311 | 3 | 0.104 | 1.200 | 0.307 | <0.001 |
| Light probe*Bumpiness*Material*Convexity | 0.668 | 3 | 0.223 | 2.580 | 0.052 | <0.001 |
| Position*Light probe*Bumpiness*Material*Convexity | 0.126 | 3 | 0.042 | 0.490 | 0.692 | <0.001 |
| Error | 491.436 | 5696 | 0.086 | | | |
| Total | 654.316 | 5759 | | | | |

Post-hoc test: Tukey HSD (Refraction (RI = 1.51) vs other 3 surface materials)

| Fig2.3A |
|---|
| p (vs matte) = 1 |
| p (vs specular) < 0.001 |
| p (vs refraction (50%) + specular (50%)) < 0.001 |

| Fig2.3B |
|---|
| **Eucalyptus Grove - smooth** |
| p (vs matte) = 1 |
| p (vs specular) < 0.001 |
| p (vs refraction (50%) + specular (50%)) < 0.001 |
| **Eucalyptus Grove - Bumpy** |
| p (vs matte) = 0.005 |
| p (vs specular) < 0.001 |
| p (vs refraction (50%) + specular (50%)) = 0.251 |
| **St Peters Basilica - smooth** |
| p (vs matte) < 0.001 |
| p (vs specular) < 0.001 |
| p (vs refraction (50%) + specular (50%)) < 0.001 |
| **St Peters Basilica - Bumpy** |
| p (vs matte) = 0.957 |
| p (vs specular) = 1 |
| p (vs refraction (50%) + specular (50%)) = 0.783 |

| Fig2.3C |
|---|
| p (vs matte) = 1 |
| p (vs specular) < 0.001 |
| p (vs refraction (50%) + specular (50%)) < 0.001 |

| Fig2.3D |
|---|
| **Eucalyptus Grove - smooth** |
| p (vs matte) = 0.420 |
| p (vs specular) = < 0.001 |
| p (vs refraction (50%) + specular (50%)) = < 0.001 |
| **Eucalyptus Grove - Bumpy** |
| p (vs matte) = 0.002 |
| p (vs specular) < 0.001 |
| p (vs refraction (50%) + specular (50%)) = 0.567 |
| **St Peters Basilica - smooth** |
| p (vs matte) < 0.001 |
| p (vs specular) < 0.001 |
| p (vs refraction (50%) + specular (50%)) < 0.001 |
| **St Peters Basilica - Bumpy** |
| p (vs matte) = 1 |
| p (vs specular) = 1 |
| p (vs refraction (50%) + specular (50%)) = 1 |

Post-hoc test: Tukey HSD (Matte vs other 3 surface materials)

| Fig2.3A |
| --- |
| p (vs refraction (RI = 1.51)) = 1 |
| p (vs specular) < 0.001 |
| p (vs refraction (50%) + specular (50%)) < 0.001 |

| Fig2.3B |
| --- |
| **Eucalyptus Grove - smooth** |
| p (vs refraction (RI = 1.51)) = 1 |
| p (vs specular) < 0.001 |
| p (vs refraction (50%) + specular (50%)) < 0.001 |
| **Eucalyptus Grove - Bumpy** |
| p (vs refraction (RI = 1.51)) = 0.005 |
| p (vs specular) = 0.457 |
| p (vs refraction (50%) + specular (50%)) = 1 |
| **St Peters Basilica - smooth** |
| p (vs refraction (RI = 1.51)) < 0.001 |
| p (vs specular) < 0.001 |
| p (vs refraction (50%) + specular (50%)) < 0.001 |
| **St Peters Basilica - Bumpy** |
| p (vs refraction (RI = 1.51)) = 0.957 |
| p (vs specular) = 1 |
| p (vs refraction (50%) + specular (50%)) = 1 |

| Fig2.3C |
| --- |
| p (vs refraction (RI = 1.51)) = 1 |
| p (vs specular) < 0.001 |
| p (vs refraction (50%) + specular (50%)) < 0.001 |

| Fig2.3D |
| --- |
| **Eucalyptus Grove - smooth** |
| p (vs refraction (RI = 1.51)) = 0.420 |
| p (vs specular) < 0.001 |
| p (vs refraction (50%) + specular (50%)) < 0.001 |
| **Eucalyptus Grove - Bumpy** |
| p (vs refraction (RI = 1.51)) = 0.002 |
| p (vs specular) = 0.639 |
| p (vs refraction (50%) + specular (50%)) = 0.998 |
| **St Peters Basilica - smooth** |
| p (vs refraction (RI = 1.51)) < 0.001 |
| p (vs specular) < 0.001 |
| p (vs refraction (50%) + specular (50%)) < 0.001 |
| **St Peters Basilica - Bumpy** |
| p (vs refraction (RI = 1.51)) = 1 |
| p (vs specular) = 1 |
| p (vs refraction (50%) + specular (50%)) = 1 |